International Journal of Engineering (IJE)

ISSN : 1985-2312

VOLUME 4, ISSUE 4

PUBLICATION FREQUENCY: 6 ISSUES PER YEAR

International Journal of Engineering (IJE)

Volume 4, Issue 4, 2010

Edited By
Computer Science Journals
www.cscjournals.org

Editor in Chief Dr. Kouroush Jenab

International Journal of Engineering (IJE)

Book: 2010 Volume 4, Issue 4

Publishing Date: 30-10-2010

Proceedings

ISSN (Online): 1985-2312

IJE Journal is a part of CSC Publishers

http://www.cscjournals.org

Published in Malaysia

Typesetting: Camera-ready by author, data conversation by CSC Publishing Services – CSC Journals, Malaysia

CSC Publishers

Editorial Preface

This is the fourth issue of volume four of International Journal of Engineering (IJE). The Journal is published bi-monthly, with papers being peer reviewed to high international standards. The International Journal of Engineering is not limited to a specific aspect of engineering but it is devoted to the publication of high quality papers on all division of engineering in general. IJE intends to disseminate knowledge in the various disciplines of the engineering field from theoretical, practical and analytical research to physical implications and theoretical or quantitative discussion intended for academic and industrial progress. In order to position IJE as one of the good journal on engineering sciences, a group of highly valuable scholars are serving on the editorial board. The International Editorial Board ensures that significant developments in engineering from around the world are reflected in the Journal. Some important topics covers by journal are nuclear engineering, mechanical engineering, computer engineering, electrical engineering, civil & structural engineering etc.

The coverage of the journal includes all new theoretical and experimental findings in the fields of engineering which enhance the knowledge of scientist, industrials, researchers and all those persons who are coupled with engineering field. IJE objective is to publish articles that are not only technically proficient but also contains information and ideas of fresh interest for International readership. IJE aims to handle submissions courteously and promptly. IJE objectives are to promote and extend the use of all methods in the principal disciplines of Engineering.

IJE editors understand that how much it is important for authors and researchers to have their work published with a minimum delay after submission of their papers. They also strongly believe that the direct communication between the editors and authors are important for the welfare, quality and wellbeing of the Journal and its readers. Therefore, all activities from paper submission to paper publication are controlled through electronic systems that include electronic submission, editorial panel and review system that ensures rapid decision with least delays in the publication processes.

To build its international reputation, we are disseminating the publication information through Google Books, Google Scholar, Directory of Open Access Journals (DOAJ), Open J Gate, ScientificCommons, Docstoc and many more. Our International Editors are working on establishing ISI listing and a good impact factor for IJE. We would like to remind you that the success of our journal depends directly on the number of quality articles submitted for review. Accordingly, we would like to request your participation by submitting quality manuscripts for review and encouraging your colleagues to submit quality manuscripts for review. One of the great benefits we can provide to our prospective authors is the mentoring nature of our review process. IJE provides authors with high quality, helpful reviews that are shaped to assist authors in improving their manuscripts.

Editorial Board Members
International Journal of Engineering (IJE)

Editorial Board

Table of Content

Volume 4, Issue 4, October 2010

Pages

Error Probability of Different Modulation Schemes for OFDM based WLAN standard IEEE 802.11a

Sanjeev Kumar sanjeev_be@indiatimes.com
Asst. Professor/ Electronics & Comm. Engg./
Amritsar college of Engg. & Technology, Amritsar,
143001, India

Swati Sharma swati.719@gmail.com
M.Tech Scholar/Electronics & Comm. Engg./
Amritsar college of Engg. & Technology, Amritsar,
143001, India

Abstract

Orthogonal Frequency Division Multiplexing (OFDM) is a key technique for achieving high data rates and spectral efficiency requirements for wireless communication systems. This paper presents a modeling and simulation of OFDM based on WLAN standard (IEEE 802.11a). Performance of OFDM is evaluated for different modulation schemes such as PSK, QAM, DQPSK, and OQPSK. The performance of OFDM is compared in terms of BER vs SNR for different modulation formats.

Keywords: Additive white Gaussian noise (AWGN), QAM, OQPSK, and DPSK.

1. INTRODUCTION

Wireless Local Area Networks (WLAN) and the exponential growth of the Internet have resulted in an increased demand for new methods of obtaining high capacity wireless networks. OFDM is a modulation scheme that allows digital data to be efficiently and reliably transmitted over a radio channel, even in multipath environments [1, 2, 3]. In OFDM, the digital data is sent using many carriers, each of a different frequency and these carriers are orthogonal to each other. All these carriers transmit in unison using synchronized time and frequency, forming a single block of spectrum. OFDM has found its application in a number of wireless and wireline systems. OFDM has been adopted into several European wireless communications applications such as the digital audio broadcast (DAB) and terrestrial digital video broadcast (DVB-T) systems [4, 5]. In the United States, OFDM has been adopted in multipoint multichannel distribution services (MMDS).Both wireless LAN applications-using standards such as IEEE 802.11a and the new European Telecommunications Standard Institute's (ETSI) HiperLAN/2 specification have also installed OFDM as the modulation scheme[6,7].

Most WLAN systems currently use the IEEE802.11b standard, which provides a maximum data rate of 11 Mbps. Newer WLAN standards such as IEEE802.11a and HiperLAN2 are based on OFDM technology and provide a much higher data rate of 54 Mbps. However systems of the near future will require WLANs with data rates of greater than 100 Mbps, and so there is a need to further improve spectral efficiency and data capacity of OFDM systems in WLAN applications [8]. One of the main reasons for using OFDM for Wireless LANs is relatively small amount of delay spread encountered in such applications [9].

The paper presents the performance comparison results of the various digital modulation techniques for OFDM in WLAN standard IEEE802.11a so as to obtain the most efficient modulation technique for the same.

Digital data is transferred in an OFDM link by using a modulation scheme on each subcarrier. A modulation scheme is a mapping of data words to a real (In phase) and imaginary (Quadrature) constellation, also known as an IQ constellation. For example 64-QAM (Quadrature Amplitude Modulation) has 64 IQ points in the constellation, constructed in a square with 8 evenly spaced columns in the real axis and 8 rows in the imaginary axis. The number of bits that can be transferred using a single symbol corresponds to log2 (M), where M is the number of points in the constellation, thus 64-QAM transfers 6 bits per symbol. Each data word is mapped to one unique IQ location in the constellation.

Differential Phase Shift Keying (DPSK) is the most common method of sending differential information. Instead of mapping data to an absolute phase angle, as in the case of coherent modulation, DPSK maps the data to a phase difference between symbols. For example, for differential QPSK each symbol transmits 2 bits of information, corresponding to 4 different phase differences.

2. OFDM GENERATION AND RECEPTION

OFDM signals are typically generated digitally. Figure 1 shows the block diagram of a typical OFDM transceiver. The transmitter section converts digital data to be transmitted, into a mapping of subcarrier amplitude and phase by using modulation techniques. It then transforms this spectral representation of the data into the time domain using an Inverse Fast Fourier Transform as it is much more computationally efficient, and so is used in all practical systems [10, 11]. The addition of a cyclic prefix to each symbol solves both ISI and ICI [12, 13, 14]. If the channel impulse response has a known length L, the prefix consists simply of copying the last L-1 values from each symbol and appending them in the same order to the front of the symbol. Digital data is then converted to serial form and transmitted over the channel.

After the time-domain signal passes through the channel, it is broken back into the parallel symbols and the prefix is simply discarded. The receiver performs the reverse operation of the transmitter. The amplitude and phase of the subcarriers is then picked out and converted back to digital data.

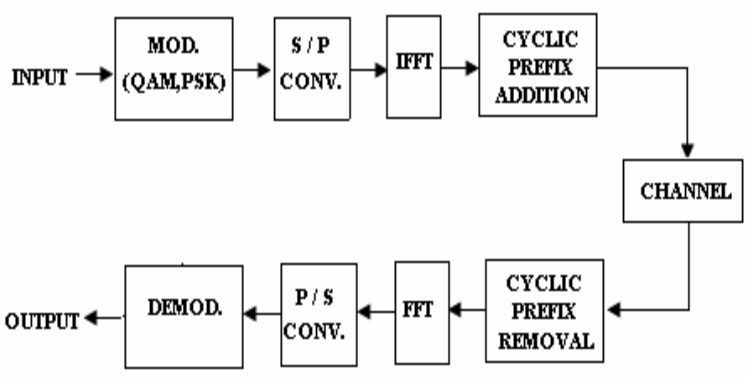

FIGURE 1: Block diagram showing a basic OFDM transceiver

When an OFDM transmission occurs in a multipath radio environment, frequency selective fading can result in groups of subcarriers being heavily attenuated, which in turn can result in bit errors.

3. SIMULATION RESULTS

OFDM for WLAN IEEE 802.11a system using different modulation schemes in the presence of AWGN and Rayleigh fading channel was simulated using Matlab. The OFDM signal parameters for the system are given in table 1.

Channel Spacing	IFFT	No. of Subcarriers	Carrier Spacing (Fc)
20 MHz	64	52	312.5 kHz (=20 MHz/64)

TABLE 1: Simulation Parameters

Two different types of subcarrier modulation i.e. Coherent and Differential (for M=2, 4, 16) are used. In addition to these, OQPSK is also used. The results presented show the BER performance as a function of the channel SNR. In log scale the SNR for a given Eb/No can be found with:

$$E_s/N_o dB = E_b/N_o dB + 10*\log_{10}(nSC/nFFT) + 10*\log_{10}(Td/Td + Tc) + 10*\log_{10}(k)$$

Where

nSC is No. of subcarriers
Tc is cyclic prefix duration
Td is Data symbol duration
Ts is Total Symbol duration and k equals $\log_2$ (M).

The graphs of BER vs Eb/No for Coherent PSK, QAM, OQPSK and DPSK for M=4 in AWGN channel are shown in figure 2 whereas figure 3 shows BER for same modulation techniques with M=16 in AWGN channel.Similarly the graphs of BER verses Energy per bit to Noise ratio for PSK, DPSK, OQPSK (M=2, 4, 16) in Rayleigh channel are shown in figure 4.

The SNR for each modulation takes into account the number of bits per symbol, and so the signal power corresponds to the energy per bit times the number of bits per symbol. The higher Eb/No required for transferring data means that more energy is required for each bit transfer.

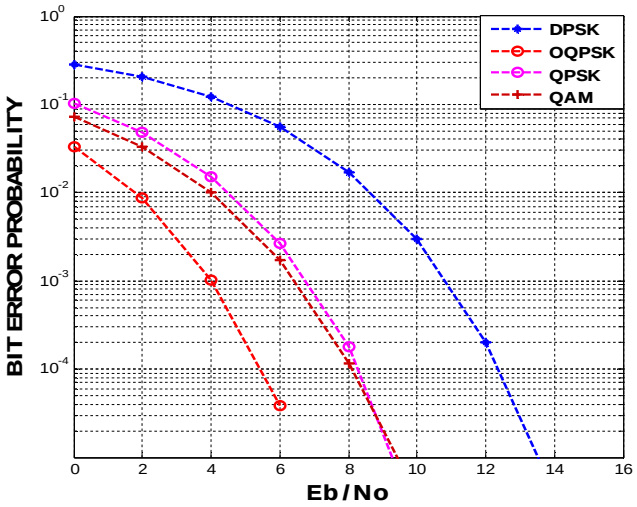

FIGURE 2: BER vs SNR for AWGN channel (M=4)

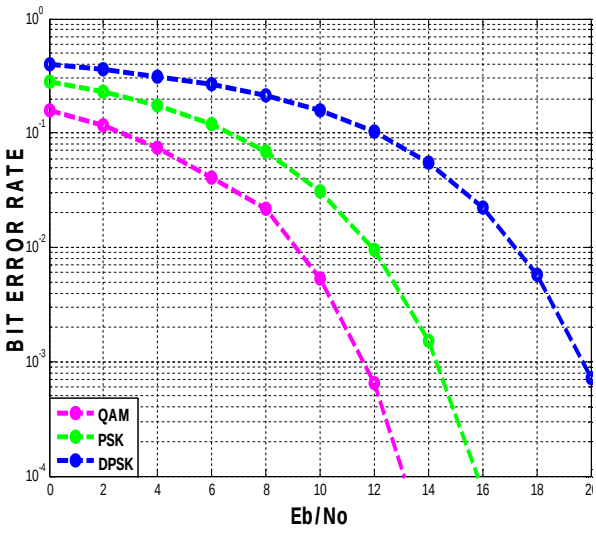

FIGURE 3: BER vs SNR for AWGN channel (M=16)

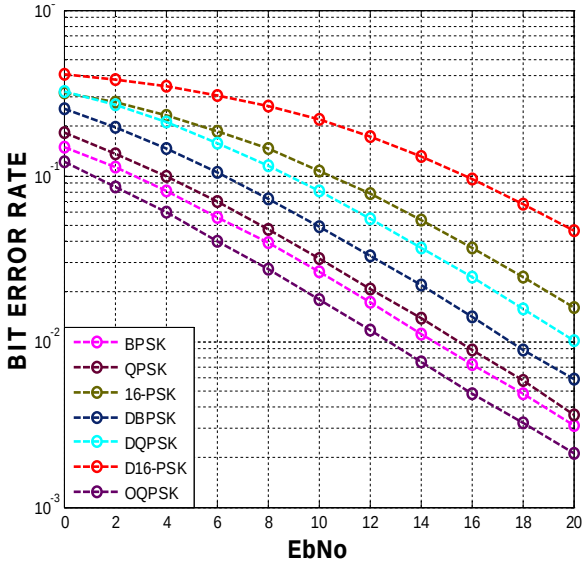

FIGURE 4: BER vs SNR for Rayleigh channel using PSK, DPSK, and OQPSK (M=2, 4, and 16)

4. CONCLUSION

All wireless communication systems use modulation schemes to map the information signal to a form that can be effectively transmitted over the communication channel.

We presented a performance study of M-ary modulation schemes viz. PSK, OQPSK, QAM and DPSK for FFT-OFDM technique using the system parameters for WLAN standard (IEEE 802.11a).The performance analysis of the WLAN system is based on BER versus SNR for above mentioned modulation formats in Additive white guassian noise channel and the Rayleigh fading channel which is one of the channel scenarios as found in most of the wireless applications.

The SNR for each modulation takes into account the number of bits per symbol, and so the signal power corresponds to the energy per bit times the number of bits per symbol. The higher Eb/No required for transferring data means that more energy is required for each bit transfer.

From the performed simulations, it was found that in AWGN channel, Coherent QAM performs best in that it shows the least bit error rate requiring the least SNR for M=16 while differential PSK is the worst for the same value of M. Whereas for M = 4, OQPSK performs the best as it requires least SNR and DPSK performs the worst in AWGN channel.
Similarly, for Rayleigh channel, OQPSK modulation done on the transmitted bits performs the best of all the other modulation techniques i.e. PSK and DPSK for the various values of M. The low efficiency of PSK in AWGN channel is a result of under utilization of the IQ vector space. As it is a known fact that PSK only uses the phase angle to convey information, with amplitude being ignored, QAM uses both amplitude and phase for information transfer and so is more efficient than PSK in AWGN channel for an OFDM system.

5. REFERENCES

[1] J. Chuang and N. Sollenberger, "*Beyond 3G: Wideband wireless data access based on OFDM and dynamic packet assignment*," IEEE Communications Mag., vol. 38, pp. 78–87, July 2000.

[2] Saltzberg, B. R., "*Performance of an Efficient Parallel Data Transmission System*," IEEE Trans. on Communications, Vol. COM-15, No. 6, December 1967, pp. 805–811.

[3] A.G.Armada, "*Understanding the Effects of Phase Noise in OFDM*," IEEE Transaction on Broadcasting, vol. 47, No.2, June 2001.

[4] STOTT, J.H., "*The DVB terrestrial (DVB-T) specification and its implementation in a practical modem"*. In proceedings of the 1996 International Broadcasting Convention, IEEE Conference Publication No. 428, pp. 255-260, September 1996.

[5] Sari, Karam, Jeanclaude," Transmission techniques for digital terrestrial TV broadcasting", IEEE communications magazine Vol.33,No.2,Feb.1995.

[6] Ahmad R.S. Bahai and Burton R. Saltzberg. "*Multicarrier digital communications, theory and applications of OFDM",* Kluwer Academic Publishers, pp. 192 (2002)

[7] ETSI,"Hiperlan/2-TechnicalOverview",Online: http://www.etsi.org/technicalactiv/Hiperlan/hiperlan2tech.htm

[8] T. Pollet, M. van Bladen, and M. Moeneclaey, *"BER sensitivity of OFDM systems to carrier frequency offset and Wiener phase noise,"* IEEE Trans. Commun., vol. 43, pp. 191–193, Feb./Mar./Apr. 1995.

[9] S. Glisic. *"Advanced Wireless Communications, 4G Technology"*. John Wiley & Sons Ltd: Chichester, 2004.

[10] L. Hanzo, W. Webb, and T. Keller, "*Single and Multi-carrier Quadrature Amplitude Modulation*", New York, USA: IEEE Press-John Wiley, April 2000.

[11] S. B. Weinstein and P. M. Ebert, "*Data transmission by frequency division multiplexing using the discrete fourier transform*," IEEE Transactions on Communication Technology, vol. COM–19, pp. 628–634, October 1971.

[12] K. Fazel and G. Fettweis, eds., "*Multi-Carrier Spread-Spectrum"*. Dordrecht: Kluwer, 1997. ISBN 0-7923-9973-0.

[13] X. Cai and G. B. Giannakis, "*Low-complexity ICI suppression for OFDM over time- and frequency-selective Rayleigh fading channels*," in Proc. Asilomar Conf. Signals, Systems and Computers, Nov. 2002.

[14] Shaoping Chen and Cuitao Zhu, "*ICI and ISI Analysis and Mitigation for OFDM Systems with Insufficient Cyclic Prefix in Time-Varying Channels***"** IEEE Transactions on Consumer Electronics, Vol. 50, No. 1, February 2004.

[15] J.A.C. Bingham, "*Multicarrier Modulation for Data Transmission: an idea who's time has come*", IEEE Communications Magazine, Vo1.28, No.5, pp.5-14, May 1990.

A Comparison of Correlations for Heat Transfer from Inclined Pipes

Krishpersad Manohar kmanohar@eng.uwi.tt
Department of Mechanical and Manufacturing Engineering
The University of the West Indies St. Augustine,
Trinidad and Tobago
West Indies

Kimberly Ramroop kimberlyramroop@gmail.com
Department of Mechanical and Manufacturing Engineering
The University of the West Indies St. Augustine,
Trinidad and Tobago
West Indies

Abstract

A review of literature on heat transfer coefficients indicated very little work reported for cross-flow pipe arrangement at various angles of inclination. In this study forced airflow at 1.1 m/s and 2.5 m/s across 2 steel pipes of diameters 0.034m and 0.049m were examined with pipe orientation inclined at 30 and 60 degrees to the horizontal position. A comparison of the experimentally determined $N\overline{u}$ and the conventional method using existing correlations for horizontal pipes in cross-flow showed that at 30 degrees inclination, 1.1 m/s, $N\overline{u}$ values were in good agreement. However, there were large differences at 60 degrees inclination, 2.5 m/s. Comparing experimental data with the correlations of Churchill, Zhukaukas, Hilpert, Fand and Morgan showed that for 30 degrees inclination the deviation from experimental $N\overline{u}$ at 1.1 m/s ranged from 2% to 18% and 2% to 8% for the 0.034m and 0.049m pipes, respectively, while at 2.5 m/s the deviation ranged from 12 % to 31% and 20% to 41% for the 0.034m and 0.049m diameter pipes, respectively. At 60 degrees inclination the deviation from experimental $N\overline{u}$ at 1.1 m/s ranged from 19% to 45% and 27 % to 41% for the 0.034m and 0.049m pipes, respectively, while at 2.5 m/s the deviation ranged from 48% to 65% and 29% to 52% for the 0.034m and 0.049m diameter pipes, respectively.

Keywords: Convective heat transfer, Inclined pipes, Heat transfer correlations.

1. INTRODUCTION

In the study of thermodynamics the average heat transfer coefficient, $\overline{h}$, is used in calculating the convection heat transfer between a moving fluid and a solid. This is the single most important factor for evaluating convective heat loss or gain. Knowledge of $\overline{h}$ is necessary for heat transfer design and calculation and is widely used in manufacturing processes, oil and gas flow processes and air-conditioning and refrigeration systems. The heat transfer coefficient is critical for designing and developing better flow process control resulting in reduced energy consumption and enhanced energy conservation. Application of external flow forced convection heat transfer coefficient range from the design of heat exchangers and aircraft bodies to the study of forced convection over pipes.

With the continued increase in design complexity and the modernization of process plant facilities, the study of forced convection over cylindrical bodies has become an important one [1].
By the formulation of correlations, which consist of dimensionless parameters, such as *Nusselt* number (*Nu*), *Reynold's* number (Re) and *Prandtl* number (Pr), for different geometries, the values of $\bar{h}$ can be calculated without having to analyze experimental data in every possible convective heat transfer situation that occurs. Dimensionless numbers are independent of units and contain all of the fluid properties that control the physics of the situation and involve one characteristic length. It is advantageous to present data in the form of dimensionless parameters since it extends the applicability of the data. However, correlations using dimensionless numbers are developed for particular geometries and situations and are applicable within that range. Therefore, it is impractical to use correlations developed for horizontal pipes to determine the $\bar{h}$ for inclined pipes.

2. PRESENTLY USED CORRELATIONS

Presently there are many correlations to predict the heat transfer from heated vertical or horizontal pipes in both forced and natural convection situations. A review of literature on heat transfer coefficients indicated that very little experimental work has been done on inclined pipes in the recent past with little or no conclusive work reported for cross-flow pipe arrangement at various angles of inclination. Generally, for design purposes cross flow correlations for horizontal pipes are being used to determine heat transfer coefficients for inclined orientation. Few correlations exist for inclined pipes with natural convection and none exist for inclined pipes in forced convection flow. Following is a brief overview of the most common correlations that are being used for a horizontal pipe in cross-flow.

2.1 Hilpert

Hilpert [2] was one of the earliest researchers in the area of forced convection from heated pipe surfaces. He developed the correlation:

$$\bar{Nu}_D = \left(\frac{\bar{h}D}{k} \right) = C \, \mathrm{Re}_D^m \, \mathrm{Pr}^{\frac{1}{3}} \qquad (1)$$

TABLE I. HILPERT'S CONSTANTS FOR FORCED CONVECTION

Re_D	C	m
0.4-4	0.981	0.33
4-40	0.911	0.385
40-4000	0.683	0.446
4000-400,000	0.193	0.618
400,000-40,000,000	0.027	0.805

where the values of *C* and *m,* are given on Table I.

Hilpert's calculations were done using integrated mean temperature values, not mean film temperature values, and with inaccurate values for the thermophysical properties of air. The thermal conductivity values of air used by Hilpert were lower (2-3%) than the most recent published results [3]. This resulted in the values of *Nusselt* number calculated by the Hilpert correlation to be higher than they should be.

2.2 Fand and Keswani

Fand and Keswani [4, 5] reviewed of the work of Hilpert and recalculated the values of the constants *C* and *m* in equation 1 using more accurate values for the thermophysical properties of air. The constants proposed by Fand and Keswani are given on Table II.

TABLE II. FAND'S CONSTANTS

Re_D	C	m
1-4	-	-
4-35	0.795	0.384
35-5000	0.583	0.471
5000-50000	0.148	0.633
50000-230000	0.0208	0.814

2.3 Zuakaukas

Another correlation proposed by Zukaukas [6] for convective heat transfer over a heated pipe was

$$Nu_f = c\,\mathrm{Re}_f^m\,\mathrm{Pr}_f^{0.37}\left(\mathrm{Pr}_f / \mathrm{Pr}_w\right)^{0.25} \tag{2}$$

where the values of *c* and *m* are given on Table III. Except for Pr_w, all calculations were done at the mean film temperature.

TABLE III. ZUAKAUKAS' CONSTANTS

Re_D	C	m
1-40	0.76	0.4
40-10^3	0.52	0.5
10^3-2(10)^5	0.26	0.6
2(10)^5-10^7	0.023	0.8

2.4 Churchill and Bernstein

Churchill and Bernstein [7, 8] proposed a single comprehensive equation that covered the entire range of Re_D for which data was available, as well as a wide range of Pr. The equation was recommended for all Re_D.Pr > 0.2 and has the form

$$Nu_D = 0.3 + \frac{0.62\,\mathrm{Re}_D^{1/2} + \mathrm{Pr}^{1/3}}{\left[1 + \left(0.4/\mathrm{Pr}\right)^{2/3}\right]^{1/4}}\left[1 + \left(\frac{\mathrm{Re}_D}{282{,}000}\right)^{5/8}\right]^{4/5} \tag{3}$$

This correlation was based on semi-empirical work and all properties were evaluated at the film temperature.

2.5 Morgan

Morgan [9] conducted an extensive review of literature on convection from a heated pipe and proposed the correlation

$$\bar{Nu}_D = \left(\frac{\bar{h}D}{k}\right) = C\,\mathrm{Re}_D^m\,\mathrm{Pr}^{\frac{1}{3}} \tag{4}$$

where the values of *C* and *m* are given on Table IV.

TABLE IV. MORGAN'S CONSTANTS

Re_D	C	m
0.0001-0.004	0.437	0.0895
0.004-0.09	0.565	0.136
0.09-1	0.800	0.280
1-35	0.795	0.384
35-5000	0.583	0.471
5000-50000	0.148	0.633
50000-200000	0.0208	0.814

3. EXPERIMENTAL PROCEDURE

3.1 Test Apparatus

A low velocity circular cross-section wind tunnel was designed and built to experimentally determine $\bar{h}$ for circular pipes in cross flow arrangement at varying angles of inclination to the horizontal. The apparatus was designed to accommodate test specimen centrally across the diameter of the wind tunnel as shown in Figure 1(a). The wind tunnel test section was 1.5 m in diameter and 3 m long after which the tunnel was tapered to a diameter of 1 m to accommodate the attachment of a 1 m diameter variable speed extractor fan, Figure 1(b). In this arrangement the wind flowed transversely across the test specimen. The wind tunnel was constructed from 3 mm thick galvanized steel sheet and reinforced with an outer wooden frame.

(a) (b)

Figure1. Photograph of test apparatus

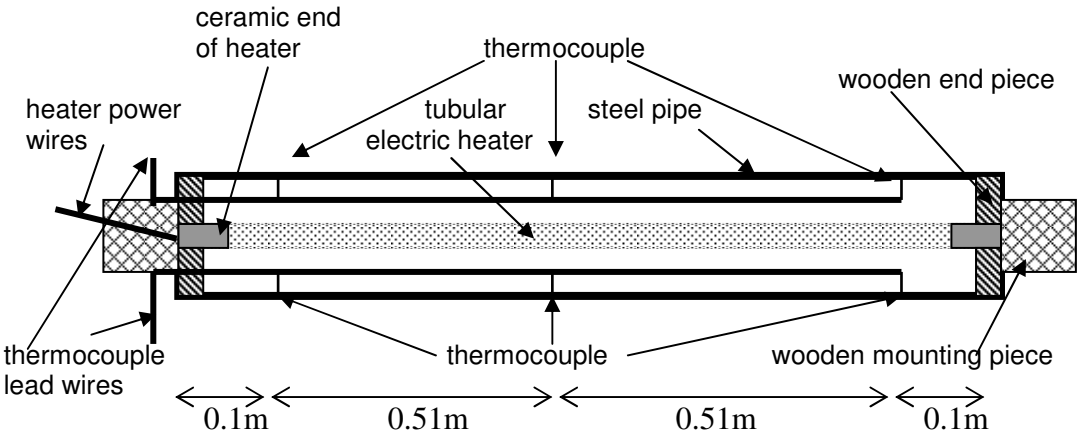

Figure 2. Schematic of test specimen

3.2 Test Specimen

Two test specimens of outer diameter 0.034 m and 0.049 m were prepared from standard schedule 40 steel pipes. The test specimens were 1.22 m long with a 1.07 m long, 0.012 m diameter electric

tubular heater centrally located inside the pipes as shown in Figure 2. Six thermocouples were placed at the outer surface of the pipes. The thermocouples lead wires were passed through the annular space and the thermocouple fixed at the pipe outer surface through holes drilled at the appropriate locations. The test pieces were respectively centrally suspended and rigidly fixed with the wooden mounting pieces diagonally across the wind tunnel at a distance of 0.75 m from the leading edge. The circular section test chamber allowed the inclination angle of the test specimens to be varied easily.

3.3 Temperature Measurement

The pipe surface temperature was monitored with the Pico TC-08 data logger via K-type thermocouples. With K-type thermocouples the TC-08 has a resolution of 0.025 ^{o}C and an accuracy of 0.3% over the temperature range –120 ^{o}C to 1050 ^{o}C. The six thermocouples were strategically located on the pipe surface as show in Figure 2. To check for uniform pipe surface temperature and surface temperature stability preliminary heating tests were conducted to verify the test arrangement. Equilibrium conditions were approached within 30 minutes of heating and were verified by subsequently monitoring the six thermocouples at 5 seconds time intervals for twenty minutes. Equilibrium conditions were taken as being established when the variation in temperature readings from the six thermocouples over a twenty-minute period was within 0.75 %. The fluctuation with individual temperature readings were < 0.2 % over the equilibrium twenty-minute period. A plot of one set of temperature readings for the 0.034m and the 0.049m diameter pipes at 75^{o} orientation to the horizontal with no fan (zero air velocity) is shown on Figure 3.

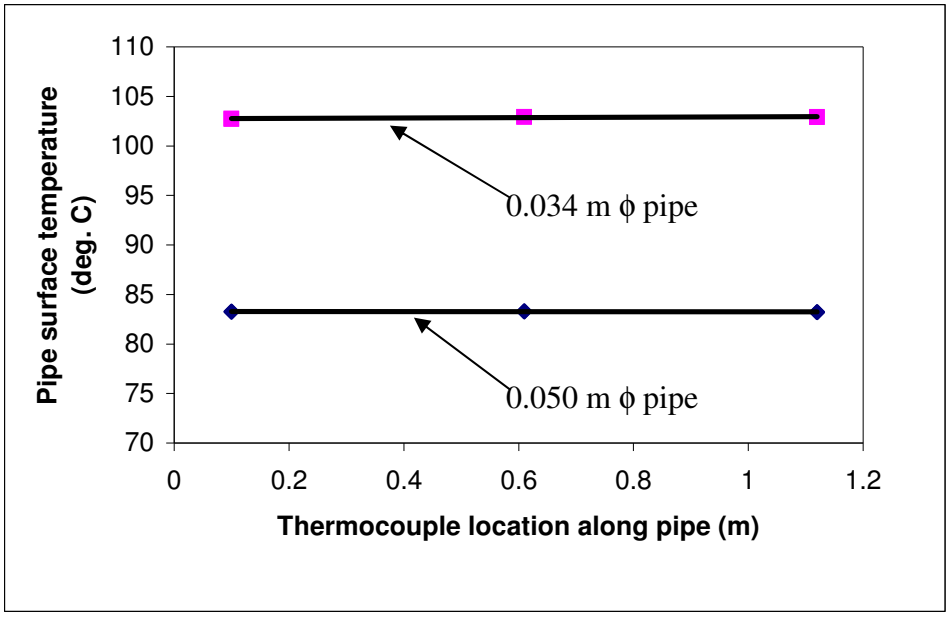

Figure 3. A plot of one set of temperature readings for pipes at 75^{o} orientation to the horizontal with no fan (zero air velocity).

3.4 Test Procedure

The speed of the extractor fan was first adjusted to provide the target air velocity in the wind tunnel. The electric heater was then powered at 90 W. The power was supplied and monitored by the MICROVIP MK1 energy analyzer. The accuracy of the primary measurements (voltage and current) of this instrument is 1%. The apparatus was continuously monitored (temperature readings were recorded at 5 s intervals) with preliminary measurements to determine uniformly heated pipe surface, airflow stability and establishment of equilibrium conditions. After equilibrium, temperature readings were recorder for ten minutes and the average values over this ten-minute period calculated as the experimental result for the test. The power was then switched off and the test pipe allowed to cool to room temperature. This procedure was repeated three times for each test

variation and the average of the three test results was calculated and used to determine the heat transfer coefficient, $\overline{h}$.

3.5 Tests Conducted

For the 0.034 m and the 0.049 m diameter pipes tests were conducted at 0, 15, 30, 45, 60, 75 and 90 degrees inclination to the horizontal for air flow velocities of 0.00 m/s, 0.80 m/s, 1.35 m/s and 2.50 m/s, for every case. For each test, after establishing equilibrium conditions, data for the pipe surface temperature, wind tunnel wall temperature, ambient air temperature, wind speed across the test specimen and power to the heater were recorded. The respective experimentally determined heat transfer coefficient, $\overline{h}$ **,** was calculated for every case and the *Nusselt* number, $N\overline{u}$, determined.

4. CALCULATIONS

The measured power input to the heater was taken as the total heat loss from the pipe surface under equilibrium conditions. The radiative heat loss component was calculated and the convective heat loss component was then determined from equation (5). The average heat transfer coefficient, $\overline{h}$ **,** was then calculated from the convective heat transfer component of equation (5).

$$Q_{total} = Q_{conv} + Q_{rad} = \overline{h}\pi DL(T_s - T_\infty) + \varepsilon\sigma\pi DL\left(T_s^4 - T_{surr}^4\right) \quad (5)$$

The $\overline{h}$ was then used to determine the average *Nusselt* number, $N\overline{u}$, from equation (6).

$$N\overline{u} = \frac{\overline{h}D_o}{k} \quad (6)$$

Where $N\overline{u}$ = average *Nusselt* number
$\overline{h}$ = average heat transfer coefficient (W/m^{2}K)
k = thermal conductivity of fluid (air) (W/m.K)
D_0 = pipe outer diameter (m)

The $N\overline{u}$ was also calculated for the corresponding test conditions with the commonly used correlations of Hilpert, Fand and Keswani, Zukaukas, Churchill and Bernstein, and Morgan. The calculated results are given on Table V.

4.1 Experimental Uncertainty

The experimental $N\overline{u}$ was calculated from equation (6) using the experimentally determined *h* from equation (5). The value of *h* depends on the measured power (voltage and current) and measured temperature values. From equations (5) and (6) the relationship for the experimentally determined $N\overline{u}$ is given by equation (7).

$$N\overline{u} = \frac{Q_{total} - Q_{rad}}{\pi DL(T_s - T_\infty)}\left(\frac{1}{k}\right)D = \frac{W - \varepsilon\sigma(T_s^4 - T_{surr}^4)}{\pi DL(T_s - T_\infty)}\left(\frac{1}{k}\right) \quad (7)$$

From the theory of uncertainty analysis [10, 11]the uncertainty in experimentally determined *Nusselt* number, $\frac{\Delta N\overline{u}}{N\overline{u}}$, from the relation in equation (7) is given by equation (8)

$$\frac{\Delta N\overline{u}}{N\overline{u}} = \frac{\Delta W}{W} + 5\frac{\Delta T_s}{T_s} + 4\frac{\Delta T_{surr}}{T_{surr}} + \frac{\Delta T_\infty}{T_\infty} = \frac{\Delta W}{W} + 10\frac{\Delta T}{T} \quad (8)$$

Also, the error associated with the power, ΔW, is

W = Voltage (V) X Current (I)

$$\frac{\Delta W}{W} = \frac{\Delta V}{V} + \frac{\Delta I}{I} \quad = 1\% + 1\%$$

Where:

W	=	Energy Meter Reading (W)
V	=	Voltage (V)
I	=	Current (A)
T_s	=	Surface Temperature (^oC)
T_{surr}	=	Surrounding Temperature (^oC)
T_∞	=	Ambient Air Temperature (^oC)
ΔNu	=	Error associated with Nu
ΔW	=	Error associated with MICROVIP MK1
ΔT	=	Error associated with Pico TC-08

For values of $\frac{\Delta W}{W}$ = 2% and $\frac{\Delta T}{T}$ = 0.3%, the uncertainty in experimentally determined *Nusselt* number is

$$\frac{\Delta N\overline{u}}{N\overline{u}} = \frac{\Delta W}{W} + 10\frac{\Delta T}{T} = 2\% + 10(0.3\%) = 5\%$$

TABLE V. CALCULATED NUSSELT NUMBER
0.034 m diameter pipe

Angle of Inclination from horizontal	Air Speed (m/s)	Experimental Results		Free Correlations			Forced Correlations				
		h Experimental	Nu Experimental	Nu Churchill	Nu Morgan	Nu Fand	Nu Churchill	Nu Zhukaukas	Nu Hilpert	Nu Morgan	Nu Fand
0	0.00	9.82	**11.43**	8.45	9.25	8.98	1.04	0.00	0.00	0.00	0.00
	0.80	13.02	**15.45**	8.08	8.86	8.61	22.21	19.60	15.47	17.83	17.83
	1.35	18.60	**22.57**	7.60	8.36	8.12	29.53	26.86	19.94	23.31	23.31
	2.50	24.55	**30.13**	7.19	7.93	7.70	41.07	38.83	32.22	32.61	32.61
15	0.00	9.44	**11.00**	8.57	9.37	9.10	1.04	0.00	0.00	0.00	0.00
	0.80	12.45	**15.07**	8.15	8.94	8.68	22.54	19.69	15.49	17.85	17.85
	1.35	18.09	**22.15**	7.64	8.40	8.16	29.54	26.90	19.94	23.30	23.30
	2.50	23.65	**29.05**	7.27	8.01	7.78	41.13	38.76	32.24	31.43	31.43
30	0.00	9.21	**10.72**	8.60	9.40	9.13	1.04	0.00	0.00	0.00	0.00
	0.80	11.68	**13.90**	8.33	9.13	8.86	22.25	19.89	15.49	17.86	17.86
	1.35	17.31	**20.99**	7.73	8.50	8.25	29.50	26.97	19.93	23.30	23.30
	2.50	22.34	**27.33**	7.33	8.07	7.84	40.91	38.85	32.07	31.40	31.40
45	0.00	9.21	**10.71**	8.58	9.39	9.12	1.04	0.00	0.00	0.00	0.00
	0.80	11.68	**13.52**	8.41	9.21	8.94	22.28	19.99	15.50	17.87	17.87
	1.35	16.85	**20.42**	7.79	8.56	8.31	29.57	26.97	23.30	23.20	23.20
	2.50	21.42	**26.30**	7.60	8.20	7.97	41.08	39.16	32.23	31.56	31.56
60	0.00	9.15	**10.63**	8.59	9.39	9.12	1.04	0.00	0.00	0.00	0.00
	0.80	11.58	**13.73**	8.33	9.12	8.86	22.20	19.85	15.51	17.82	17.82
	1.35	16.72	**20.51**	7.83	8.60	8.35	29.55	27.12	19.95	23.33	23.33
	2.50	21.22	**26.06**	7.48	8.25	7.99	41.11	39.20	32.17	31.56	31.56
75	0.00	9.12	**10.60**	8.60	9.40	9.13	1.04	0.00	0.00	0.00	0.00
	0.80	11.44	**13.55**	8.33	9.13	8.87	22.15	19.82	15.43	17.78	17.78
	1.35	16.65	**20.24**	7.84	8.62	8.32	29.56	27.16	19.96	23.33	23.33
	2.50	21.10	**25.87**	7.47	8.22	7.95	41.04	39.13	32.18	31.51	31.51
90	0.00	9.09	**10.52**	8.57	9.38	9.11	1.04	0.00	0.00	0.00	0.00
	0.80	11.57	**13.69**	8.30	9.09	8.83	22.15	19.72	15.42	17.77	17.77
	1.35	16.30	**19.83**	7.87	8.64	8.39	29.54	27.14	19.91	23.25	23.25
	2.50	20.85	**25.50**	7.47	8.21	7.98	40.92	39.02	32.06	31.43	31.43

CALCULATED NUSSELT NUMBER
0.049 m diameter pipe

Angle of Inclination from horizontal	Air Speed (m/s)	Experimental Results		Free Correlations			Forced Correlations				
		h Experimental	Nu Experimental	Nu Churchill	Nu Morgan	Nu Fand	Nu Churchill	Nu Zhukaukas	Nu Hilpert	Nu Morgan	Nu Fand
0	0.00	9.46	**16.69**	10.99	11.81	11.67	1.04	0.00	0.00	0.00	0.00
	0.80	11.99	**21.45**	10.52	11.35	11.02	27.62	24.85	19.97	21.91	21.91
	1.35	17.59	**32.00**	9.73	10.55	10.25	36.74	34.01	28.22	28.51	28.51
	2.50	23.24	**42.63**	9.16	9.97	9.68	51.32	59.22	41.79	41.24	41.24
15	0.00	9.30	**16.40**	11.01	11.83	11.48	1.04	0.00	0.00	0.00	0.00
	0.80	11.92	**21.33**	10.55	11.37	11.04	27.63	24.87	18.75	21.91	21.91
	1.35	17.17	**31.23**	9.79	10.62	10.31	36.73	34.04	24.12	28.51	28.51
	2.50	22.39	**41.11**	9.26	10.07	9.78	51.37	49.35	41.84	41.29	41.29
30	0.00	9.27	**16.29**	10.98	11.80	11.46	1.04	0.00	0.00	0.00	0.00
	0.80	11.46	**20.40**	10.57	11.39	11.06	27.46	24.74	18.82	21.79	21.79
	1.35	17.09	**30.97**	9.76	10.58	10.28	36.60	33.90	24.05	28.41	28.41
	2.50	22.12	**40.45**	9.24	10.05	9.76	51.14	49.11	41.62	41.07	41.07
45	0.00	9.23	**16.22**	11.01	11.83	11.48	1.04	0.00	0.00	0.00	0.00
	0.80	11.37	**20.24**	10.60	11.43	11.09	27.48	24.78	18.72	21.80	21.80
	1.35	16.90	**30.20**	9.81	10.64	10.33	36.67	34.00	24.09	28.02	28.02
	2.50	21.76	**39.58**	9.20	10.01	9.72	50.80	48.67	41.03	40.75	40.75
60	0.00	9.16	**16.02**	10.93	11.75	11.41	1.04	0.00	0.00	0.00	0.00
	0.80	11.13	**19.69**	10.55	11.38	11.05	27.29	24.58	18.60	21.66	21.66
	1.35	16.48	**29.70**	9.77	10.59	10.28	36.37	33.62	23.91	28.24	28.24
	2.50	21.21	**38.49**	9.23	10.04	9.75	50.67	48.67	41.18	40.63	40.63
75	0.00	9.05	**15.89**	11.01	11.86	11.49	1.04	0.00	0.00	0.00	0.00
	0.80	11.11	**19.69**	10.60	11.42	11.09	27.35	24.67	18.64	21.71	21.71
	1.35	16.32	**29.60**	9.83	10.65	10.34	36.51	33.87	23.99	28.35	28.35
	2.50	20.81	**37.88**	9.32	10.13	9.84	50.85	48.70	41.35	40.79	40.79
90	0.00	8.91	**15.57**	11.01	11.83	11.49	1.04	0.00	0.00	0.00	0.00
	0.80	11.05	**19.57**	10.59	11.42	11.09	27.32	24.63	18.61	21.68	21.68
	1.35	16.25	**29.20**	9.85	10.68	10.37	36.46	33.83	23.96	25.31	25.31
	2.50	20.39	**37.07**	9.35	10.17	9.87	50.71	48.86	41.28	40.72	40.72

5. DISCUSSION

The test apparatus designed for determination of $\bar{h}$ functioned on the fundamental principle of an energy balance when equilibrium conditions were established. Due to the lack of published data for mixed convective heat loss from inclined pipes comparison of the experimental findings with similar published work was limited. Under the circumstances, the experimentally determined $N\bar{u}$ was compared with the $N\bar{u}$ calculated from the commonly used correlations of Hilpert, Fand and Keswani, Zukaukas, Churchill and Bernstein, and Morgan on Table 5.

For all test conditions the Morgan and Fand correlations yielded the same $N\bar{u}$. A comparison of the experimentally determined $N\bar{u}$ and the conventional method using existing correlations for horizontal pipes in cross-flow showed that at 30^o inclination, 1.1 m/s, $N\bar{u}$ values were generally in good agreement. For this condition the 0.034 m and 0.049m diameter pipes showed maximum and minimum deviation of 18% and 1%, and 8% and 2%, respectively. The largest differences occurred with the 60^o inclination, 2.5 m/s. For this condition the 0.034 m and 0.049m diameter pipes showed maximum and minimum deviation of 65% and 48%, and 52% and 29%, respectively. For the 30^o, 2.5 m/s condition the 0.034 m and 0.049m diameter pipes showed maximum and minimum deviation of 31% and 12%, and 41% and 20%, respectively. For the 60^o, 1.1 m/s condition the 0.034 m and 0.049m diameter pipes showed maximum and minimum deviation of 45% and 19%, and 41% and 27%, respectively.

The results on Table 5 indicate that as air velocity increased, the differences between experimental values of $N\bar{u}$ and values obtained from the correlations for horizontal cylinders in cross-flow also increased. The experimental results showed that as the angle of inclination increased, the $N\bar{u}$ decreased, indicating reduced overall heat transfer from the surface as expected. However, the calculated values of $N\bar{u}$ from the published correlations do not show this expected trend. Therefore, the use of correlations developed for forced convection from horizontal pipes to calculate $\bar{h}$ for inclined pipes under forced airflow conditions, especially if the angle of inclination from the horizontal position is large, will result in erroneous results.

6. CONCLUSIONS

- There is an urgent need for the formulation of correlations for convective heat transfer under mixed flow conditions with inclined pipe orientation.
- The study shows that the use of horizontal pipe correlations for calculating heat loss from inclined pipe orientation yields erroneous results of significant magnitude.
- Designers and engineers need to be guided when using horizontal pipe correlations for inclines pipe calculations as there may be significant errors.

7. WORK IN PROGRESS

At present work is being done with pipes oriented at 15^o, 30^o, 45^o, 60^o, 75^o and 90^o to the horizontal. Tests are being conducted at three low speed air velocities, to determine the effect of forced airflow on the heat transfer from the surface of the inclined pipe.

8. REFERENCES

1. Jisheng Li and J. Tarasuk. “Local Free Convection Around Inclined Cylinders in Air: An Interferometric Study,” Experimental Thermal and Fluid Science, 5:235-242. 1992.
2. Hilpert, R. “Heat Transfer from Cylinders,” Forsch. Geb. Ingenieurwes, 4:215. 1933.
3. Incropera F. and D. De Witt. Fundamentals of Heat and Mass Transfer, 5th Edition, USA. 2002.

4. Fand, R. M. and K. K. Keswani. “A Continuous Correlation Equation for Heat Transfer from Cylinders to Air in Crossflow for Reynold’s Numbers from 10^{-2} to $2(10)^5$,” International Journal of Heat and Mass Transfer, 15:559-562. 1972.
5. Fand, R.M. and K. K. Keswani. “Recalculation of Hilpert’s Constants,” Transactions of ASME, pp. 224-226. 1973.
6. Zukauskas, A. “Heat Transfer From Tubes in Crossflow,” Advances in Heat Transfer, 8:87-159. 1987.
7. Churchill, S.W. and H. H. S. Chu. “Correlating Equations for Laminar and Turbulent Free Convection From a Horizontal Cylinder,” International Journal of Heat And Mass Transfer, 18:1049-1053. 1975.
8. Churchill, S. W. and M. Bernstein. “A correlating Equation for Forced Convection from Gases and Liquids to a Circular Cylinder in Crossflow,” J. Heat Transfer, 99:300-306. 1977.
9. Morgan, V. “Heat Transfer from Cylinders,” Advances in Heat Transfer, 11:199-264. 1987.
10. Manohar, K., Yarbrough, D. W. and Booth, J. R. “Measurement of Apparent Thermal Conductivity by the Thermal Probe Method,” Journal of Testing and Evaluation, 28(5):345-351. 2000.
11. Coleman, H. W. and Steller, W. G. “Experimentation and Uncertainty Analysis for Engineers,” 2nd Ed., John Wiley and Sons, New York, pp. 47-64 (1999).

Acknowledgement Of Evacuated Tube Solar Water Heater Over Flat Plate Solar Water Heater

Dharamvir Mangal mangaldharamvir1@rediffmail.com

Assistant Professor/ Mechanical Engineering
DepartmentMD University Rohtak
TITS, Bhiwani, 127021
Haryana, India

Devander Kumar Lamba lambadev1@rediffmail.com

Assistant Professor/ Mechanical Engineering
DepartmentMD University Rohtak
TITS, Bhiwani, 127021
Haryana, India

Tarun Gupta tarungupta1976@yahoo.com

Assistant Professor/ Mechanical Engineering
DepartmentMD University Rohtak
NGFCET, Palwal, 124001
Haryana, India

Kiran Jhamb kiran_jhamb1@rediffmail.com

Assistant Professor/ Mechanical Engineering
DepartmentLingaya's University, Faridabad
LIMAT, Faridabad, 121002
Haryana, India

Abstract

This paper presents acknowledgement to one of the latest solar water heater which is evacuated solar water heater based on a Thermo siphon principle used for heating water for domestic purposes in household by utilizing solar radiations. As the air is evacuated from the solar tube to form a vacuum, this greatly reduces conductive and convective heat loss from the interior of tube. As a result wind and cold temperature have less effect on the efficiency of evacuated solar water heater. Result of less heat loss is fastly heating of water as compared to flat plate solar water heater/collector.

Keywords: Evacuated tube 1, Solar water heater 2, Radiations 3

1. INTRODUCTION

Solar water heaters save electricity and thus money; electricity is becoming more and more expensive; they could even turnout to be more reliable than electric power supply (at least in many parts of our country); they are clean and green and thus reflect one's commitment for preservation of environment; they are safer than electric geysers as they are located on the roof; and, if well designed, may even look good on the house top.

Solar heater is a device which is used for heating the water, for producing the steam for domestic and industrial purposes by utilizing the solar energy. Solar energy is the energy which is coming from sun in the form of solar radiations in infinite amount, when these solar radiations falls on absorbing surface, then they gets converted into the heat, this heat is used for heating the water. When numbers of evacuated tubes are used for heating the water then solar heater is called evacuated tube solar water heater. Although there are many type of solar water heater like flat –plate solar water heater, evacuated tube solar water heater, concentrated solar water heater. Flat-plate solar water heaters are being used from earlier days. Now a day, they are being replaced by evacuated tube solar water heater because of number of advantages. Concentrated solar water heaters are used when we need very high temperature water or a steam. But here we would concern only with evacuated tube solar water heater. Evacuated tube solar water heaters are mainly two types according to loop system open Circuit, non-pressurized system, close Circuit, pressurized system.

2. DESCRIPTION OF EVACUATED TUBE SOLAR WATER HEATER (OPEN TYPE, NON PRESSURISED)

Main components of evacuated tube solar water heater **(**open Circuit, non-pressure system)

- Evacuated glass tubes and Barium Getter
- Storage tank
- Mounting frame
- External water supply source

FIGURE 1: Evacuated glass tubes

2.1 Evacuated glass tubes and Barium Getter

Figure1 shows the Structure of evacuated glass tube is similar to a Dewar flask which has a double wall with a vacuum between the walls. Each evacuated tube consists of two glass tubes made from extremely strong borosilicate glass with high chemical and thermal shock resistance. The outer tube is transparent allowing light rays to pass through with minimal reflection. The outer side of the inner tube is coated with a sputtered solar selective coating (Al-N/Al or AlN/AlN-SS/Cu) which features excellent solar radiation absorption and minimal reflection properties.
The top of the two tubes are fused together and the air contained in the annular space between the two layers of glass is evacuated to eliminate conductive and convective heat loss. This is why the tubes are able to absorb the energy from infrared rays which can pass through clouds. Wind and low temperatures also have less of effect on the function of evacuated tubes when compared to flat plate solar collectors due to the insulating properties of the vacuum. The top end of these parallel tubes is fitted in to the inner storage tank.

In the process of pulling the vacuum, a Barium Getter is inserted into the base of the outer glass tube. The inner glass tube is then inserted into the outside tube with the Getter centering the inner glass tube.

The Glass Tubes are heated to a high temperature, and the vacuum is pulled. The two glass tubes are then fused together at the open end. The Barium Getter also serves another purpose. When the glass tubes are heated before the ends are fused together the Barium Getter also becomes very hot and emits a pure layer of Barium at the bottom of the tube which will look like a chrome plate on the inside of the outer glass tube. If in the future, the glass becomes fractured or broken, the shiny chrome look will change to a milky colour, thus, making it easy to see if the vacuum has been lost in a particular glass tube. The barium layer also provides a clear visual indicator of the vacuum status.

2.2 Storage tank

It is a tank which stores the water and come from external water source like water tank. It is mainly consist of two tank i.e. inner tank and outer tank. The inner tank is placed inside the outer tank. The gap is maintained between two tanks. This gap is filled by high tech insulating material (Rock Wool or mineral wool) in order to reduce the heat losses from the heated water exist inside the inner tank heated by the evacuated tube solar water heater. Rock wool is a man made fiber and has many excellent characters like non-combustible, non-toxic, low thermal conductivity, long service life and so on. Storage tank is placed at the top of frame and tubes. The top open end of the tubes is connected to the storage tank. The bottom end of tubes is placed in a holder provided at bottom of the frame. A complete model of evacuated tube solar water heater **(**open Circuit, non-pressure system) is shown in figure2.

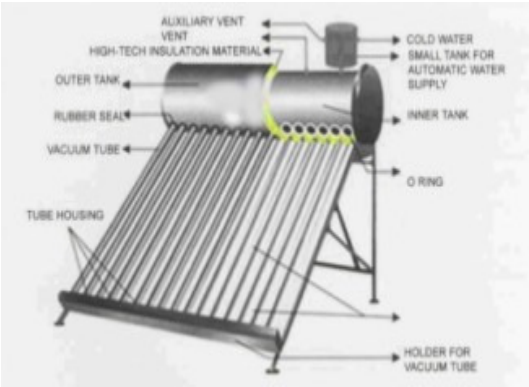

FIGURE 2: Evacuated tube solar water heater

2.3 Mounting frame

It is structure made of no. of metallic angle or plate, on which no. of units like storage tank (in case of open circuit), manifold box, tubes etc. are mounted.

2.4 External water supply source

It supplies the water to the storage tank of evacuated tube solar water heater.

2.4.1 WORKING PRINCIPLE (EVACUATED TUBE SOLAR WATER HEATER)

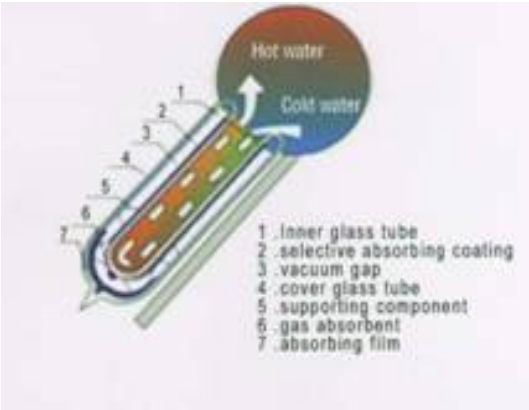

FIGURE 3: Water heating in Glass Tube

The working of evacuated solar water heater is based on a natural Principle--'Thermosiphon' as shown in figure3. The key important point of these systems is that: the storage tank is always located higher than the collector.
As the sun's rays after passing through outer glass tubes falls on the inner glass tubes which are coated with absorbent materials. So these sun's rays are absorbed by the absorbent materials and inner tube and gets converted in to heat after absorption. Due to absorption, surface of inner tubes gets heated up and this heat is transferred to the water exist inside the inner tubes. The temperature of the water in the tubes rises making it less dense or lighter and hot and lighter water naturally moves up to the top of collector and through the evacuated collector tube goes to the storage tank. This makes the colder and heavier water in water tank moves down to the bottom of the collector. That continuous displacement occurs naturally. So the users can get the hot water (30 - 90℃) from the tank. The tilt angle of these collectors varies from 15 - 90°.

2.4.2 TECHNICAL INFOMATIONS

Capacity of storage tank is depends on the water requirements used by the people. It is normally 200-250 liter for 4-5 adult people. Further technical terms are shown in Table 1 as below:

Length (Nominal)	1500 mm-1800 mm
Outer tube diameter	47 mm-58 mm
Inner tube diameter	37 mm-47 mm
Glass thickness	1.6mm-2.0mm
Material	Borosilicate glass 3.3
Absorptive coating	Graded A1/N/A1 ALN/AIN-SS/CU
Vacuum	$P < 5 \times 10^{-3}$ Pa
Thermal expansion	$3.3 \times 10^{-6}/^{0}C$
Stagnation temperature	$\geq 250^{0}C$
Absorbance (AM 1.5)	>93 %(A1/N/A1) / >96 %(ALN/AIN-SS/CU)
Emittance ($80^{0}C/176^{0}F$)	<8 %(A1/N/A1) / <5 %(ALN/AIN-SS/CU)
Heat loss	<0.8W/(m2℃)
Start up temperature	<= 25℃ (77□)

TABLE 1: Technical information

3. ADVANTAGES

When comparing peak efficiency levels it may seem that there is little difference between flat plate and evacuated tubes, in fact flat plate may actually be higher, but this is during minimal heat loss conditions. When averaged over a year evacuated tube collector have a clear advantage. The key points are:

1) Due to the cylindrical shape of the evacuated tube, the solar tubes are able to passively track the sun throughout the day. Flat plate collector only provides peak energy output at midday when the sun is perpendicular to the collector's surface.
2) Air is evacuated from the solar tube to form a vacuum. This greatly reduces conductive and convective heat loss from the interior of the tube. As a result wind and cold temperatures have less effect on the efficiency of the evacuated tube collector.
3) Lotusino solar collectors can often be used in subzero temperatures without the system sustaining damage. Flat plate systems often require expensive and complicated "antifreeze" systems to be installed.
4) Evacuated tubes are strong, long lasting, and should one be broken, inexpensive and easy to replace. If a flat plate collector panel is damaged the whole panel must be replaced.
5) Due to the high efficiency absorption of solar radiation even during overcast conditions, combined with excellent insulative properties of the solar tube, solar tube collectors can heat water all year round (backup from gas and electricity is still required).
6) Due to the various advantages of evacuated tube collector over flat plate collectors, a smaller collector can be used to provide the same heating performance. For example, a standard household of 4-5 people would usually require a 250-300L water storage tank. Depending on your location, only 30 evacuated tubes would be required to provide all summer hot water needs and a large percentage in other seasons. Flat plate solar collectors can produce similar heat output to evacuated tube collectors, but generally only during hot, sunny conditions. When averaged over an entire year, evacuated tube collector heat output per net m2 of absorber area is between 25% to 40% greater than a flat plate collector.

4. CONCLUSION

This paper introduced the benefits of evacuated tube solar water heater. In India, it is still new model of solar water heater which can be used in our household to face the challenge of climate change, global warming, energy crisis etc.

5. REFERENCES

[1] G. L. Morrison, I. Budihardjo and M. Behnia. *"Solar Energy".* 76 (1-3): 135-140, 2004

[2] I. Budihardjo, G.L. Morrison. *"Solar Energy".* 83(1): 49-56, 2009

[3] G.L. Morrison, I. Budihardjo, M. Behnia. *"Solar Energy".* 78 (2): 257-267, 2005

[4] *"Fuel and Energy Abstracts".* 45 (4): 272, 2004

[5] *"Fuel and Energy Abstracts".* 46 (6): 380, 2005

[6] G. L. Morrison, H. N. Tran. *"Solar Energy".* 33(6):515-526, 198

[7] I. Budihardjo, G. L. Morrison, M. Behnia. *"Solar Energy".* 81(12):1460-1472, 2007

Design and Simulation of a soft switching scheme for a dc-dc Boost Converter with pi controller

X.Felix Joseph felix.jsph@gmail.com
Research scholar, PRIST University, Thanjavur,India

Dr.S.Pushpakumar spushpakumar@gmail.com
Former Principal, Govt. College of Engg., Kannur,India.

D.Arun Dominic arundominicniu@yahoo.com
Lecturer,EEE dept., Noorul Islam University, Kumaracoil,India.

D.M.Mary Synthia Regis Prabha regisprabha@gmail.com
Assistant Professor,EEE dept.,Noorul Islam University, Kumaracoil,India.

Abstract

This paper presents the design of simple but powerful soft switching scheme for a DC-DC Boost Converter with a closed loop control. A new novel soft switching scheme is proposed with a single switch and minimum components which offers load independent operations. The only switch used in this converter is switched ON at zero current and switched OFF at zero voltage .The proposed Controller is used to improve the dynamic performance of DC-DC converter by achieving a robust output voltage against load disturbances. The duty cycle of the Boost converter is controlled by PI Controller. A 50W/50KHz soft switched PWM Boost converter is simulated and analyzed. The results are simulated using PSIM.

Keywords: Boost converter, Zero voltage switching, Zero current transition, Pulse Width Modulation, PI controller.

1. INTRODUCTION

Switched-mode Power Supply Units in domestic products such as personal computers often have universal inputs, meaning that they can accept power from most mains supplies throughout the world, with rated frequencies from 50 Hz to 60 Hz and voltages from 10 V to 240V. PWM based switched mode power supplies are used in telecommunication, aerospace application etc. The switches used in these types of power supplies are subjected to high switching stresses and high switching power loss that increases linearly with the switching frequency of the PWM. Hence the converters in the SMPS are also experience high switching losses, reduced reliability, electromagnetic interference and acoustic noise. Another significant drawback of the switch mode operation is the EMI produced due to large di/dt and dv/dt caused by a switch-mode operation. These shortcomings of switch-mode converters are overcome by increasing the switching frequency in order to reduce the converter size and weight and hence to increase the power

density. Therefore, to realize high switching frequency in a converter changes its status (from on to off), when the voltage across it and/or the current through it is zero at the switching instant.[3]. DC-DC converters are nonlinear systems due to their inherent switching operation. To assure a constant output voltage, a classical linear design of a control is frequently used. The regulation is normally achieved by the pulse width modulation (PWM) at a fixed frequency. The switching device is a power MOSFET. The PWM linear control techniques are widely used [8].A number of circuits [l], [2] and [5] use an additional switch to accomplish the function of soft switching the main device. The circuits proposed in [2] and [4] use a single switch but the device count is high. The circuit of accomplishes reduced voltage and current stresses and the coupling between main and auxiliary circuit inductors significantly attenuate the duty cycle limitations [4].

The PI controller is proposed is to improve the performance of the soft switched boost converters. The duty cycle of the boost converter is controlled by PI controller. The conventional PI controllers for such converters are designed under the worst case condition of maximum load and minimum line condition. As power electronic converters are nonlinear, and also are prone to variations in its operating states over a wide range, the conventional PI controllers are to be designed to provide optimal performance as the operating point changes. To provide optimal performance at all operating conditions of the system PI controller is developed to control the duty cycle of the boost converter. PI controller is designed based on an average state space model of the classical boost DC-DC converter. Simulation of boost converter subjected to load changes is performed to demonstrate the effectiveness of the proposed controller.[9][12]

A converter topology with single switch and switching strategies discussed in this paper, which make the switch on at zero current and off at zero voltage at the given switching time. This topology applied to a dc-dc boost converter. In this paper design and simulation of linear PI controller for a soft switched dc-dc converter is discussed. The results were taken for different load disturbances.

Design and Analysis of the Proposed Converter

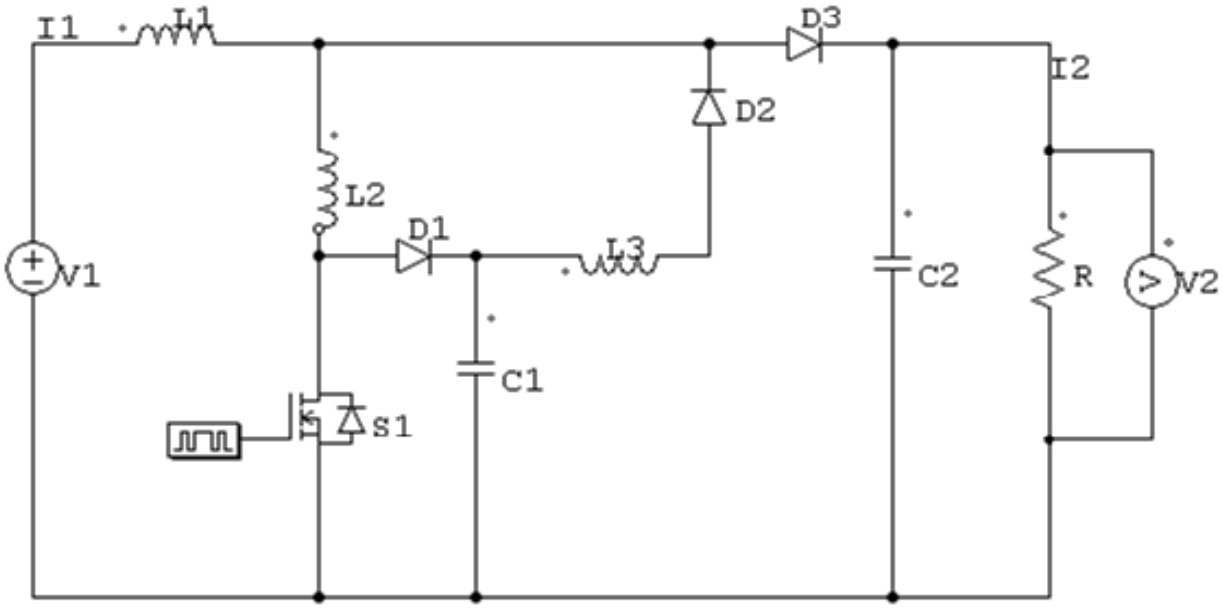

FIGURE 1: Proposed Soft switched dc-dc boost converter

The circuit diagram of the proposed converter with soft switching scheme is shown in fig.1, the switch S_1, L_1, D3 and C_2 are the main boost converter components, while R represents the resistive load on the converter. Inductor L_2, L_3, D_1, D_2 and C_1 form the auxiliary circuit for accomplishing the soft switching of S_1. Inductors L_2 and L_3 are much smaller than L_1 and C_1 is much smaller than C_2. There are seven modes of operation. The duration of modes 1, 2, 5 and 6 being quite small i_{L1} and V_{out} are assumed constant at I_1 and V_1 for modes 1 and 2, and I_2 and V_2 for modes 5 and 6 respectively.[10]

MODE 1: This mode begins with the turn on of S_1, at zero current at t_0 .The expressions are,

$$i_{L_2}(t) = \frac{V_1}{L_2} t \quad (1)$$

$$v_{C_1}(t) = [V_1 - V_{C_1}(t_0)][1 - \cos \omega_1 t] + V_{C_1}(t_0) \quad (2)$$

$$i_{L_3}(t) = [V_{C_1}(t_0) - V_1] \frac{\sin \omega_1 t}{\omega_1 L_3} \quad (3)$$

Where $\omega_1 = \frac{1}{\sqrt{L_3 C_1}}$

When D_3 stops conducting and this mode comes to an end.

MODE 2: The initial conditions on L_3, L_2 and C_1 are, $i_{L_3}(t_1)$, $i_{L_2}(t_1) + I_1$ and V_{C_1} respectively, attained at the end of
Mode 1.The expressions are,

$$V_{C_1}(t) = -V_{C_1}(t_1)[1 - \cos \omega_2 t] + \frac{i_{L_3}(t_1)}{\omega_2 C_1} \sin \omega_2 t - V_{C_1}(t_0) \quad (4)$$

$$i_{L_3}(t) = \frac{V_{C_1}(t_1)}{\omega_2 (L_2 + L_3)} \sin \omega_2 t + i_{L_3}(t_1) \cos \omega_2 t \quad (5)$$

$$i_{L_2}(t) = \frac{V_{C_1}(t_1)}{\omega_2 (L_2 + L_3)} \sin \omega_2 t + i_{L_3}(t_1) \cos \omega_2 t + I_1 \quad (6)$$

Where $\omega_2 = \frac{1}{\sqrt{(L_2 + L_3) C_1}}$

This mode comes to an end when V_{C_1} reaches zero at t_2.

MODE 3: The initial conditions on i_{L_2}, i_{L_3} and V_{C_1} for this mode $i_{L_2}(t_2), i_{L_3}(t_2)$ are zero The expression for i_{L_3} is,

$$i_{L_3}(t) = -\frac{V_S L_2}{L_1 L_2 + L_2 L_3 + L_3 L_1} t + I_{L_3}(t_2) \quad (7)$$

This mode comes to an end at t_3 when i_{L_3} reaches zero at t_3.

MODE 4: In this mode current buildup in L_1 and L_2, and Vout(t) are governed by the equations as follows.

$$i_{L_1}(t) = i_{L_2}(t) = \frac{V_S}{L_1 + L_2} t + I_1 \quad (8)$$

$$V_{out}(t) = V_1 e^{\frac{1}{RC_2}} \quad (9)$$

This mode comes to an end when S_1 is turned off at zero voltage at t_4.

MODE 5: This mode begins with the turn off of S_1 at zero voltage at t_4.The expressions are,

$$V_{C_1}(t) = V_2(1 - \cos \omega_3 t) + \frac{I_2}{\omega_2 C_1} \sin \omega_3 t \quad (10)$$

$$I_{L_2}(t) = \frac{L_2}{(L_2 + L_3)}[V_2 C_1 \sin \omega_3 t - I_2(1 - \cos \omega_3 t)] + I_2 \quad (11)$$

$$I_{L_3}(t) = \frac{L_2}{(L_2 + L_3)}[-V_2 C_1 \omega_3 \sin \omega_3 t + I_2(1 - \cos \omega_3 t)] \quad (12)$$

Where $\omega_3 = \frac{1}{\sqrt{\frac{L_2 L_3}{L_2 + L_3} C_1}}$

This mode ends when i_{L_2} reaches zero at t_6.

MODE 6: In this mode i_{L_3} reduces to zero. This mode comes to an end at t_6 when i_{L_3} becomes zero. The expression for i_{L_3} and V_{C_1} for these mode is.

$$i_{L_3} = \frac{V_{C_1}(t_5) - V_2}{L_3 \omega_1} \sin \omega_1 t + i_{L_3}(t_5) \cos \omega_1 t \quad (13)$$

$$V_{C_1}(t) = [V_{C_1}(t_5) - V_2][\cos \omega_1 t - 1] \frac{i_{L_3}(t_5)}{\omega_1 C_1} \sin \omega_1 t \quad (14)$$

MODE 7: In this mode i_{L2}, i_{L3} are zero. This mode comes to an end at t_7 when S_1 is turned on at zero current. This is the normal mode of the boost converter. The expressions are,

$$V_{out}(t) = e^{-\alpha t}[A \sin \omega_4 t + B \sin \omega_4 t] + V_S \quad (15)$$

$$i_{L_1}(t) = \frac{V_{out}(t)}{R} + e^{-\alpha t}[(-BC_2 + AC_2 \omega_4 t) \cos \omega_4 t - (AC_2 + BC_2 \omega_4) \sin \omega_4 t] \quad (16)$$

Where $\alpha = \frac{1}{2RC_2}$, $\omega_4 = \frac{1}{\sqrt{L_1 C_2}}$

$$A = \frac{I_2}{\omega_4 C_2} - \frac{V_2}{R \omega_4 C_2} + \frac{\alpha(V_2 - V_5)}{\omega_4}$$

$$B = V_2 - V_S$$

Design of PI controller

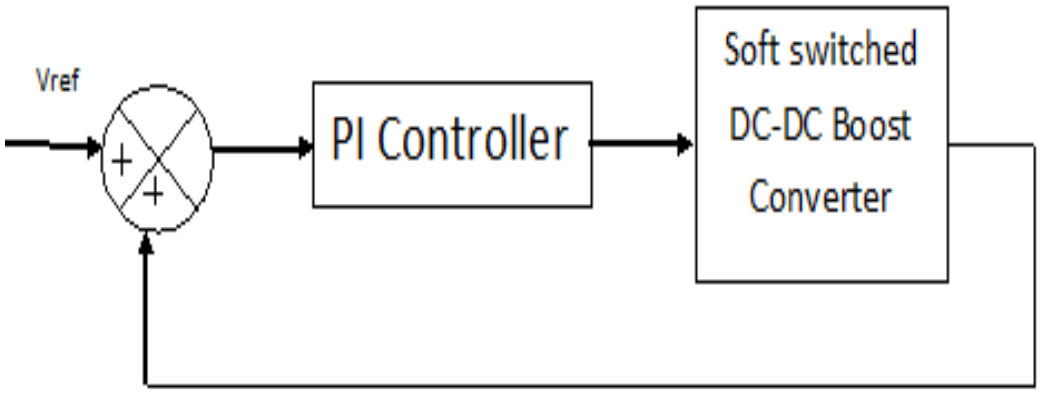

FIGURE 2: Block diagram of the Soft switched dc-dc boost converter with PI controller.

PI control is a traditional linear control method used in industrial applications. The linear PI controller controllers are usually designed for dc-dc converters using standard frequency response techniques and based on the small signal model of the converter. A Bode plot is used in the design to obtain the desired loop gain, crossover frequency and phase margin. The stability of the system is guaranteed by an adequate phase margin. However, linear PID and PI controllers can only be designed for one nominal operating point. A boost converter's small signal model changes when the operating point varies. The poles and a right-half plane zero, as well as the magnitude of the frequency response, are all dependent on the duty cycle. Therefore, it is difficult for the PID controller to respond well to changes in operating point. The PI controller is designed for the boost converter for operation during a start up transient and steady state respectively.

Fig. 2.shows the closed loop of the soft switched dc-dc boost converter with PI controller. The load current of the proposed converter is given to the PI controller. The time constant of the controller is designed according to the small signal transfer function of the boost converter which is given below. Then the output of the PI controller changes the pulse width of the square wave which changes the firing angle of the MOSFET switch, so the output of the converter is controlled for different load disturbances.

The small signal model of the boost converter is designed based on the average state space averaging techniques, the small signal transfer function of a boost converter is

$$\frac{Vo(s)}{D(s)} = \frac{Vs}{(1-D)^2} \frac{\left(1 - s\frac{L}{R(1-D)^2}\right)}{1 + s\frac{L}{R(1-D)^2} + s^2\frac{LC}{(1-D)^2}}$$

Simulation Results

For simulation purposes, a boost converter with the following specifications is used. The other parameters of the converter are L_1 =1mH, L_2=10µH, L_3= 10µH, C_1 =1µF, C2=,10pF, R=50Ω, MOSFET ('S') 'ON' resistance = 0.27 Q, and diode forward voltage drop = 1.5 V.

Input voltage	Output voltage	Rated output power	Switching frequency	Resistance
100 V	150V	50W	50Khz	50 ohms

TABLE 1: Simulation parameters

The current (fig.5) and voltage (fig.6) across the switch and the regulated output (fig.4 and fig.7),for the constant input fig.3 is studied and plotted using the PSIM. The switching behavior and performance of the proposed soft switched dc-dc boost converter for open loop and closed loop (PI controller is the feedback controller) were studied and plotted. The advantage of soft switched boost converter is that ZVS and ZCS are incorporated in the circuit.

The parameters are given as per the table1.

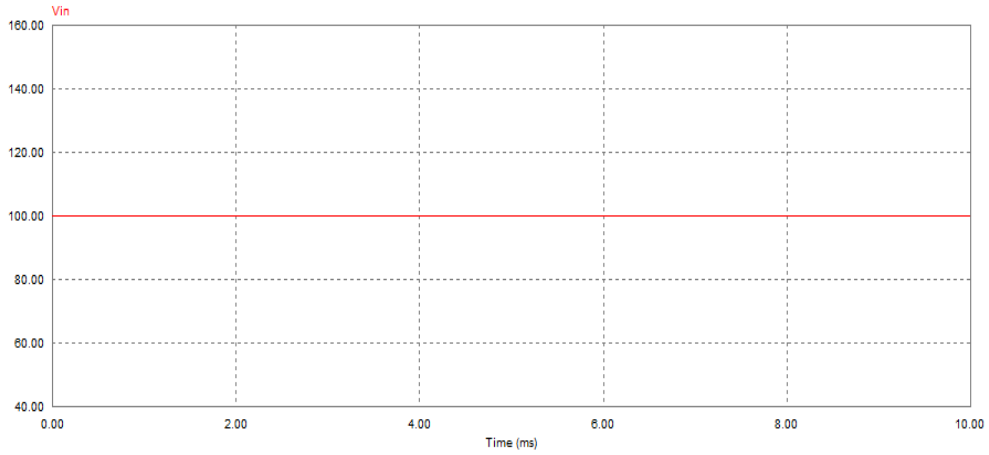

FIGURE 3: Input voltage waveform of the Soft switched dc-dc boost converter **Vin =100v**

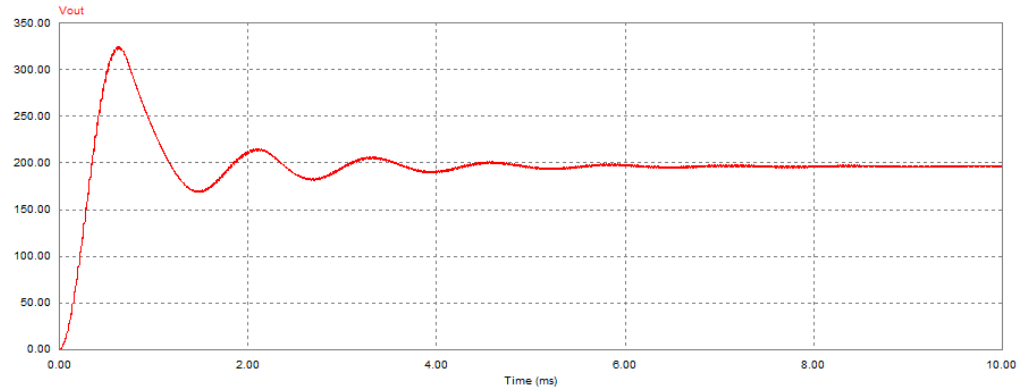

FIGURE 4: Output voltage waveform of the Soft switched dc-dc boost converter without PI controller Vout=200v

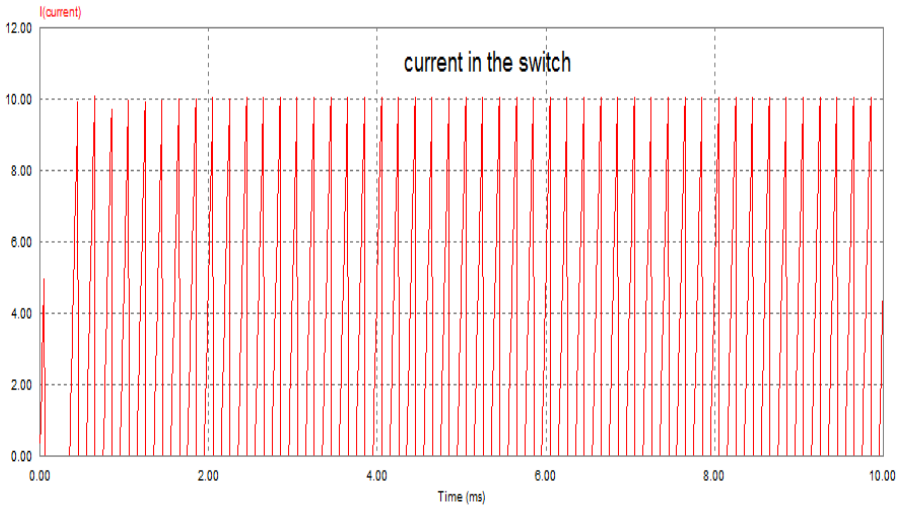

FIGURE 5: Zero current waveform of the Soft switched dc-dc boost converter.

Fig.5 and 6 shows the current and voltage waveform across the switch.Fig.4 and 7 shows the regulated output, for the constant input which is shown in fig.1.The switching behavior and performance of the proposed soft switched dc-dc boost converter for open loop and closed loop (PI controller is the feedback controller) were studied and plotted. The advantage of soft switched boost converter is that ZVS and ZCS are incorporated in the circuit. The circuit is simulated using PSIM.

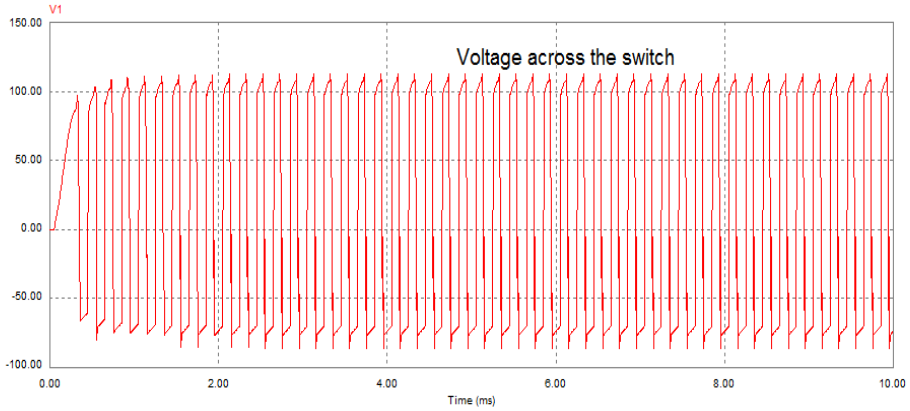

FIGURE 6: Zero Voltage waveform of the Soft switched dc-dc boost converter

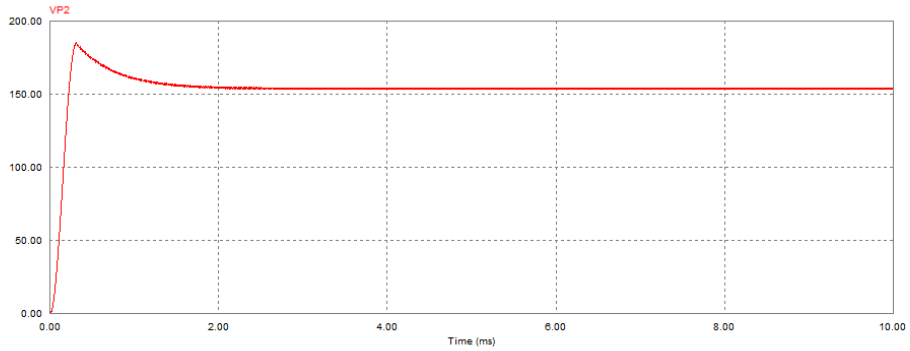

FIGURE 7: Output Voltage waveform of the proposed converter with PI controller V_{out}=150V

3. COMPARATIVE EVALUATION

Many researchers [13][14] explained soft switched dc –dc boost converter with two switches which gives high switching losses, in that one switch act as soft switching and the other as hard switching. The comparative evaluation of our results with the other research work shows that the total harmonic distortion is reduced as much as possible. Fig.8 clearly shows that the total harmonic distortion of soft switched dc-dc converter with two switches have fundamental and other odd harmonics.

Fig.9 shows that the total harmonic distortion of our proposed soft switched dc-dc converter with a single switch. It is clearly seen from the fig.9, except fundamental harmonics, higher order harmonics are eliminated, which gives the improved results over the other research works. In future we will eliminate the fundamental harmonics by using a suitable filter design techniques.

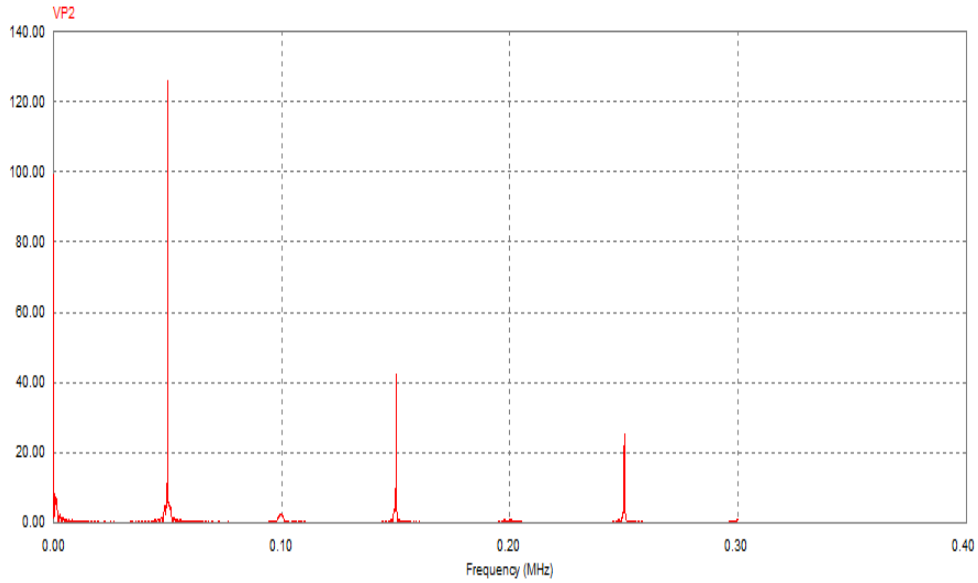

FIGURE 8: Total Harmonic Distortion of soft switched dc-dc boost converter with two switches.

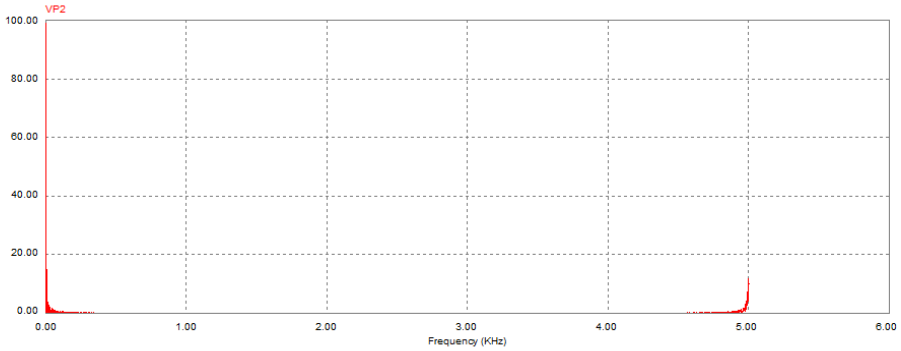

FIGURE 9: Total Harmonic Distortion of proposed soft switched dc-dc boost converter with single Switch

4.CONCLUSION & FUTURE WORK

Thus a new novel soft switching scheme is designed and simulated with a feedback control. PI controller is used for feedback control. We simulated the soft switching technique and achieved the low stress and less switching loss in the converter. The linear PI controller was designed based on frequency response of the boost converter using frequency response technique. The simulated results shows that the only switch used in this converter is switched ON at zero current and switched OFF at zero voltage. The output voltage is boosted and it is constant. It reaches the steady state vale within several micro seconds.

In future we can change the load from resistive to Inductive load or motor load. This soft switching circuit can be implemented to control different special machines like switched reluctance motor, Brushless DC motor etc. We can also change the controller to intelligent controllers like Neural network controller, fuzzy logic controller and Neuro-Fuzzy logic controller.

5. REFERENCES

1. J.A.Lambert et al" *Boost PWM converter with low voltage and current stresses*" IEEE Trans. on Power Electronics, Vol. 13,pp 26- 35 Jan 1999 .

2. K.H.Liu, R Oruganti, and F.C. Lee, "*Zero voltage switches and quasi-resonant DC-DC converters*," IEEE PESC Conf.,pp 58-70 1987.

3. Ned Mohan, M. Under land, P. Robbins. *"Power Electronics Converters, Applications and Design"*, John Willey & Sons Inc., pp. 249-295.

4. Elasser and D.A. Torry, "*Soft switching active snubber for dc/dc converters*," IEEE trans. Power Electronics, vol. 11, pp. 710-722 Sep. 96.

5. Ching-Jung Tseng and Chern-Lin Chen, "*Passive lossless snubbers for DC/DC converters"* Proceedings *of IEEE PESC* .1998, pp. 1049-1054.

6. G.Uma,M.Shanthi and C.Chellamuthu*,"Design and implementation of constant frequency soft-switched regulated power supply for aerospace applications"*, IEEE- ISIE'2000, Cholula, Puebla, Mexico.2000

7. Kwang-Hwa Liu, "*Zero-Voltage Switching Techinique in DC-DC Converters*",IEEE Transactions On Power Electronics vol-5,no-3.1990.

8. Chok-You Chan, "*A Nonlinear Control for DC-DC Power Converters*", IEEE Transaction on Power Electronics, vol. 22, No. 1, pp 216-222.2007

9. Rajani K. Mudi and Nikhil R. Pal ,(1999), "*A Robust Self-Tuning Scheme for PI-and PD-Type Fuzzy Controllers*", IEEE Transactions on fuzzy systems, vol. 7, No. 1. pp 2-15

10. M.D.Bagaewadi, B.G.Fernandes, R.V.S.Subrahmanyan, "*A Novel Soft Switched Boost Converter Using A Single Switch*". Power Electronics and Motion Control Conference.2000.

11. Aleksandar Prodic, Dragan Maksimovic and Robert W. Erickson, (2001), "*Design and Implementation of a digital PWM Controller for a High-Frequency Switching DC-DC Power Converter*", IECON'01: The 27th Annual Conference of the IEEE Industrial Electronics Society, 2001 IEEE, pp 893-898.

12. V.S.C Raviraj,P.C.Sen,"*Comparitive Study Of Proportional-Integral,Sliding Mode And Fuzzy Logic Controllers For Power Converters*",IEEE Transactions On Industrial Electronics,Vol.33.No-2,March\April 1997.

13. Jaehyuck Kim, R. Krishnan "*Novel Two-Switch-Based Switched Reluctance Motor Drive for Low-Cost High-Volume Applications*" Jaehyuck Kim, *,* and R. Krishnan, IEEE Transactions On IndustrialApplications,Vol.45,.No-4,July \August 2009.

14. Sungsik Park, Sewan Choi*," Soft-Switched CCM Boost Converters With High Voltage Gain for High-Power Applications",* IEEE Transactions On Power Electronics Vol.25,.No-45,May 2010.

15. Ying-Chun Chuang, Yu-Lung Ke, "*High – Efficiency and Low Stress ZVT-PWM DC to DC Converter for Battery Charger*" IEEE Transactions On Industrial Electronics,Vol.55.No-8,Page 3030-3037,Nov 2008.

16. S.Joseph Jawhar**,** N.S Marimuthu (2008) "*An Intelligence Controller for a non Linear power Electronic Boost Electronic Converter*" International Journal of Soft computing Techniques Vol 3 No.1 Page no. 69-73.

17. Liping Guo, John Y. Hung and R.M.Nelms, (2003), "*Digital Controller Design for Buck and Boost Converters Using Root Locus Techniques*", IEEE. pp-1864-1869.2003.

18. S.Arulselvi,Uma Govindarajan, V.Saminath, "*Development Of Simple Fuzzy Logic Controller(SFLC) for ZVS Quasi Resonant converter: Design, Simulation And Exprimentation*", Indian Institute of Science Journal May-June 2006,86,Pp 215-233.

19. Muhammad H.Rashid "*Power Electronics Circuits,Devices And Applications*."Prentice-Hall India,2004.

CFD and Artificial Neural Networks Analysis of Plane Sudden Expansion Flows

Lyes Khezzar lkhezzar@pi.ac.ae
Mechanical Engineering Department
The Petroleum Institute Abu Dhabi,
Po Box 2533, United Arab Emirates

Saleh M. Al-Alawi Saleh@squ.edu.om
Electrical Engineering Department
Sultan Qaboos University Muscat,
Al Khod, Sultanate of Oman

Abstract

It has been clearly established that the reattachment length for laminar flow depends on two non-dimensional parameters, the Reynolds number and the expansion ratio, therefore in this work, an ANN model that predict reattachment positions for the expansion ratios of 2, 3 and 5 based on the above two parameters has been developed. The R^2 values of the testing set output Xr1, Xr2, Xr3, and Xr4 were 0.9383, 0.8577, 0.997 and 0.999 respectively. These results indicate that the network model produced reattachment positions that were in close agreement with the actual values. When considering the reattachment length of plane sudden-expansions the judicious combination of CFD calculated solutions with ANN will result in a considerable saving in computing and turnaround time. Thus CFD can be used in the first instance to obtain reattachment lengths for a limited choice of Reynolds numbers and ANN will be used subsequently to predict the reattachment lengths for other intermediate Reynolds number values. The CFD calculations concern unsteady laminar flow through a plane sudden expansion and are performed using a commercial CFD code STAR-CD while the training process of the corresponding ANN model was performed using the *NeuroShell*^{TM} simulator.

Keywords: Sudden Expansion, ANN, CFD, Reattachment, Laminar flow.

1. INTRODUCTION

When a fluid is flowing through a plane sudden-expansion duct, the boundary layers separate at the expansion plane because of a singularity in the wall geometry. The separating shear layer will reattach at a downstream location that varies with the Reynolds number defined as $\mathrm{Re} = Ud/\nu$ and the expansion ratio equal to D/d, where D and d refer to the downstream and upstream duct respectively, see Figure 1. At reattachment, part of the shear layer is deflected upstream into the recirculation zone and the other part proceeds downstream as a recovering boundary layer. The behavior of such flows and especially the reattachment lengths downstream

of the expansion plane are important topics of consideration for design of fluidic devices, heat-exchangers and mixing systems.
It is known that laminar flow downstream of a sudden expansion remains symmetric with two equal separation zones on either side of the centerline of the duct for low Reynolds numbers. However, beyond a critical value of the Reynolds number the flow becomes asymmetric, producing two or three unequal separation zones. The exact underlying phenomenon is still not well understood but is thought to be due to a Coanda like phenomenon and the appearance of asymmetric flow is thought to coincide with a bifurcation of the Navier-Stokes equations. It has been found both experimentally and numerically that the value of the critical Reynolds number beyond which the flow behavior becomes asymmetric is dependent on the expansion ratio. Of particular interest in these flows, is the variation of reattachment lengths with Reynolds number and expansion ratio.

Plane sudden expansion flows have been investigated experimentally by Durst et al [1], Cherdron et al [2] and Fearn et al. [3]. These investigations included flow visualisation and fluid velocity measurements by laser Doppler anemometry. Numerical investigations were also conducted by Durst et al [1], Fearn et al [3] and Battaglia et al [4]. The techniques used were generally based on time integration by finite difference/element techniques of the incompressible form of the Navier-Stokes equations. The calculations of these flows with mesh sizes necessary to resolve the flow field, provide grid-independent solutions and to obtain the salient features of the flow for every Reynolds number can be very time consuming. For example, using a Computational Fluid Dynamic (CFD) commercial code, around 27 hours of computing time on a SUN-20 workstation, are necessary to obtain a converged solution for a single Reynolds number.

ANNs are computer models that are trained in order to recognize both linear and non-linear relationships among the input and the output variables in a given data set. In general, ANN applications in engineering have received wide acceptance. The popularity and acceptance of this technique stems from its features, which are particularly attractive for data analysis. These features include handling of fragmented and noisy data, speed inherent to parallel distributed architectures, generalization capability over new data, ability to effectively incorporate a large number of input parameters, and its capability of modeling non-linear systems. In general, ANN models consists of three basic elements: an organized architecture of interconnected processing elements, a method for encoding information during training, and a method for recalling information during testing. Simpson (1990) provides a coherent description of these elements and presents comparative analyses, applications, and implementation of 27 different ANN paradigms. This tool can be used by mechanical engineers in conjunction with other analytical and graphical techniques for data analysis, optimisation and model evaluation.

When considering the reattachment length of sudden-expansions the judicious combination of CFD calculated solutions with ANN will result in a considerable saving in computing and turnaround time. Thus CFD can be used in the first instance to obtain reattachment lengths for a limited choice of Reynolds numbers and ANN will be used subsequently to predict the reattachment lengths for other intermediate Reynolds number values.

The purpose of this work is twofold. First present a CFD analysis of flows through plane sudden expansions. Second, the results of this analysis will be used in conjunction with ANN to demonstrate that the hybrid combination of ANN and CFD modelling allows a considerable time saving in the prediction of reattachment lengths for plane sudden expansions.

The next section of this paper will present the theoretical model used to obtain finite-volume solutions to the flow through plane sudden expansions chosen from previously published work. Section three presents the ANN model, the results are presented in section 4 followed by conclusions.

2. NUMERICAL SIMULATION IN PLANE SYMMETRIC SUDDEN EXPANSIONS

2.1 Model Equations and Numerical Method

The flow is assumed to be laminar, two-dimensional and unsteady, the fluid viscous and incompressible. Under these assumptions, the continuity and momentum equations are therefore written in their conservative form and for Cartesian systems of co-ordinates as:

$$\frac{\partial U}{\partial x}+\frac{\partial V}{\partial y}=0 \tag{1}$$

$$\frac{\partial (U)}{\partial t}+\frac{\partial (U^2)}{\partial x}+\frac{\partial (UV)}{\partial y}=-\frac{1}{\rho}\frac{\partial P}{\partial x}+\frac{\mu}{\rho}\left(\frac{\partial^2 U}{\partial x^2}+\frac{\partial^2 U}{\partial y^2}\right) \tag{2}$$

$$\frac{\partial (V)}{\partial t}+\frac{\partial (UV)}{\partial x}+\frac{\partial (V^2)}{\partial y}=-\frac{1}{\rho}\frac{\partial P}{\partial y}+\frac{\mu}{\rho}\left(\frac{\partial^2 V}{\partial x^2}+\frac{\partial^2 V}{\partial y^2}\right) \tag{3}$$

where, (U, V) are the fluid velocity vector Cartesian components, P represents the pressure and ρ and μ the density and viscosity of the fluid respectively.

The finite-volume technique is used to solve the above equations. The second order QUICK scheme of Leonard [5] was employed for the discretization convection fluxes and a second-order centred difference scheme was adopted for diffusive fluxes. The pressure field P is solved with the PISO algorithm, see Issa [6]. Temporal integration is achieved through a fully implicit formulation with a time step of 10^{-5}. Convergence was assumed when the global rates of change of the variables were between 10^{-10} and 10^{-11} for laminar flow and 10^{-7} for turbulent flow and monitoring of variables at relevant positions in the flow field. All the calculations were carried on a SUN-20 workstation, to 64-bits precision.

2.2 Initial-boundary conditions and meshes

The geometrical details of the configuration are shown on figure 1. The computational grid was rectangular and extended from the exit plane of the expansion to a downstream position giving a length of up to 70 step-heights.

The calculations proceeded by impulsively starting the flow from rest. At the inlet boundary, a fully developed parabolic profile was prescribed.

At the outlet plane, a zero gradient condition is enforced for all variables and this boundary was located at a downstream distance of 50 and in some instances 70 step heights. The axial length of the domain of integration was assumed to be long enough to capture the flow details and remove upstream influence of the outlet boundary face value. At solid boundaries, the usual law of the wall was used.

The mesh was rectangular with uniform distributions along the stream wise and cross-stream directions. Three grid sizes were used 150×55 and 200×93 and 250×110 to generate grid independent solutions as judged by the profiles of the axial velocity. There were no significant differences between the results of the last two grids and therefore the intermediate one was adopted in all the computations.

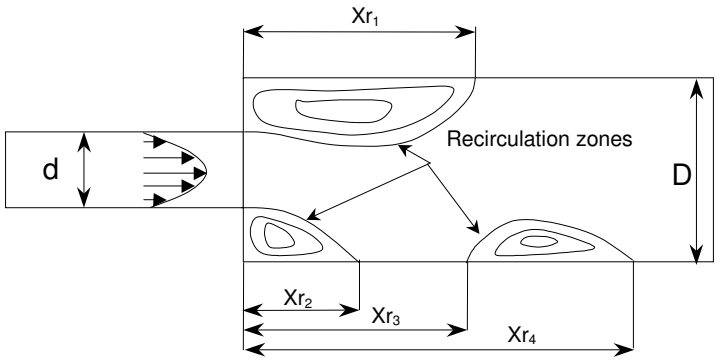

FIGURE 1: Geometrical configuration of the plane sudden-expansion.

3. ARTIFICIAL NEURAL NETWORKS MODEL

3.1 Artificial Neural Networks

An artificial neural network (ANN) method is a computational mechanism able to acquire, represent, and compute a mapping from one multivariate space of information to another, given a set of data representing that mapping. ANNs have the ability to mimic the human brain as well as their ability to learn and respond [7]. This technique found wide acceptance in various engineering applications since they have proven to be effective in performing complex operations, process and functions in a variety of fields.

An ANN can be considered as a collection of numerous simple processors organised in layers called neurons or nodes. These nodes are the basic organizational units of a neural network that are arranged in a series of layers to create the ANN by unidirectional communication channels (connections) that carry numerical data. Nodes are classified as input, output, or hidden layer nodes depending on their location and function within the network see Stern [8]. Data is received from sources external to the neural network through the input layer nodes, while data is transmitted out of the neural network through the output layer nodes. Hidden layer neurons act as the computational nodes in the neural network, communicating between input nodes and other hidden layer or output nodes. The number of nodes in the input layer is equal to the number of independent variables entered into the network which represent the input parameters whereas the number of output nodes corresponds to the number of variables to be predicted. The number of hidden layers and nodes used within the hidden layer vary according to the complexity of the task the network must perform see DeTienne et al.[9].

3.2 Model Development

It has been clearly established that the reattachment length for laminar flow depends on two non-dimensional parameters, the Reynolds number and the expansion ratio (E.R.=D/d). This dimensional analysis relationship forms the basis of the Artificial Neural Network model which is developed below.

Thus, an ANN model was developed for predicting reattachment positions for the expansion ratios of 2, 3 and 5. The ANN Architecture for this model is shown in Figure 2. The model consists of three layers, an input layer, a hidden layer and an output layer. The neurones in the input layer receive two input representing the Reynolds number (Re) and the Expansion ratios (E.R.); hence, two neurones were used for input in the ANN architecture. The output layer, on the other hand, consists of four neurones representing the reattachment positions (Xr1, Xr2, Xr3, and Xr4 of figure 1). The single hidden layer used consisted of 5 neurones. The initial number

of nodes used in the single hidden layer was calculated using the equation developed by Carpenter and Hoffman [10]:

$$N = \eta\left[H(I+1) + n(H+1)\right] \tag{4}$$

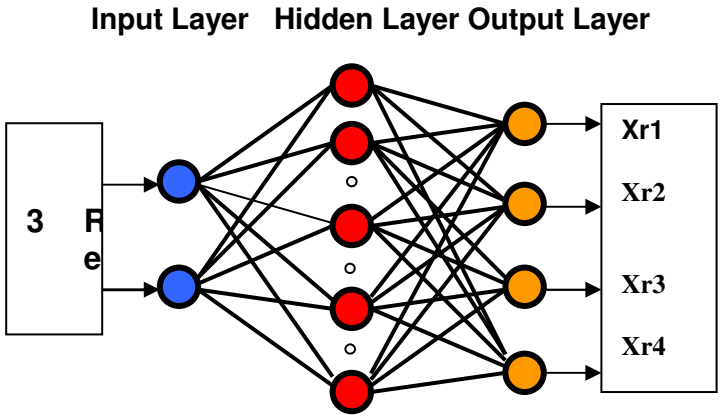

FIGURE 2: The Architecture for the Developed ANN Model.

Where, η is a constant greater than 1.0 (i.e. η =1.25 would give a 25% over-determined approximation, *N* the number of training pairs available, *H* the number of hidden nodes to be used in the network with one hidden Layer, *I* and n the number of input and output nodes respectively.

The result obtained using equation (4) indicated that four hidden nodes could be used in the hidden layer to develop the ANN architecture. However, the best result for the model was found with eight nodes in the hidden layer. Research in this area by Lapeds and Forber [11] and Hecht-Nielsen [12] proved that one or two hidden layers with an adequate number of neurones is sufficient to model any solution surface of practical interest

4. RESULTS

4.1 CFD results

The results of the CFD simulations are presented first. A detailed comparison with measured velocity data is conducted so as to provide the necessary confidence in other predicted flow parameters such as reattachment lengths for other values of Reynolds number.

The experimental results of Fearn et al. [3] are used in the study of the velocity profiles predictions. The heights of the upstream and downstream ducts were 4 and 12 mm respectively and the area and aspect ratios 1:3 and 8:1 respectively. Below a Reynolds number of 60, the flow was found to be symmetric.

Figure 3 illustrates detailed comparison of the calculated axial velocity profiles and their experimental counter parts, as measured by Fearn et al. [3], for several downstream positions for a Reynolds number equal to 187. The agreement between the calculated and measured profiles is excellent. The profile inside the third recirculation zone is also accurately predicted.

Figure 4 shows the predicted reattachment lengths with Reynolds number for the three expansion ratios of 2, 3 and 5. They correspond to the experimental studies and configurations of Cherdron et al [2], Fearn et al [3] and Ouwa et al [13]. The reattachment location is determined as the position where the stream wise velocity is zero at the first grid point from the wall. The trend of all the three curves reveals a symmetric flow at low values of the Reynolds number and transition to asymmetric flow occurs at a critical value of the latter. Initially, only two recirculation zones are present with a third one appearing later. The part of the curves that corresponds to symmetric flow extrapolates to a finite recirculation length at zero Reynolds number. Ouwa et al. [13] reported variations of the two first reattachment lengths (Xr1 and Xr2) with Reynolds number and their results agree remarkably well with the present calculations. The inferred values of the critical Reynolds number for the three ratios of 2, 3 and 5 are 180, 60 and 45 respectively and compare well with the experimental values of 185, 54 and 45. The source of the discrepancies is difficult to trace but can be explained in terms of difficulty in obtaining an exact value for the transitional Reynolds number.

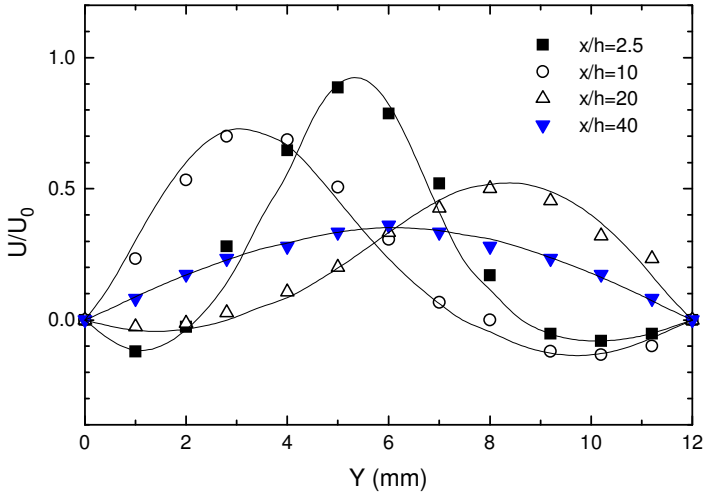

FIGURE 3: Axial Mean velocity (Fearn et al), Re=187.

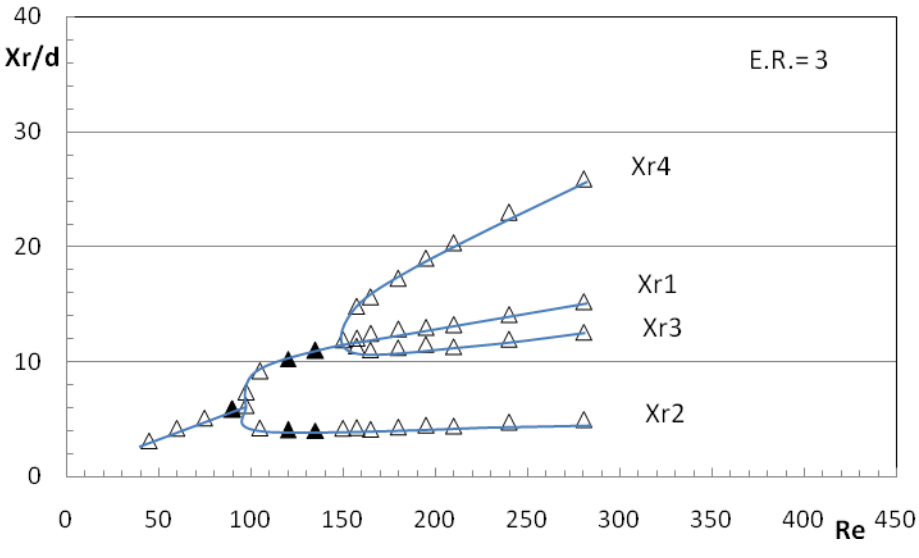

(a)

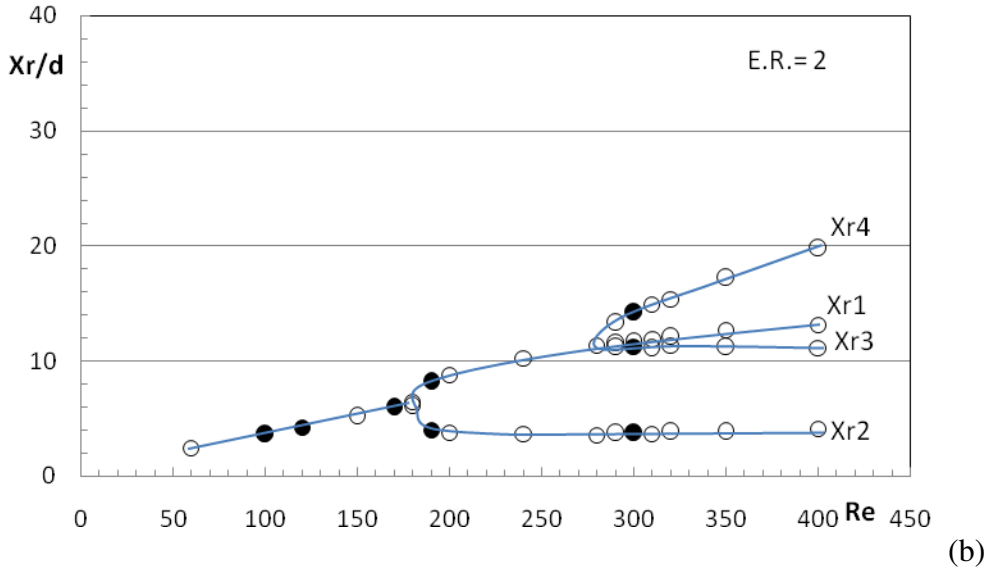

(b)

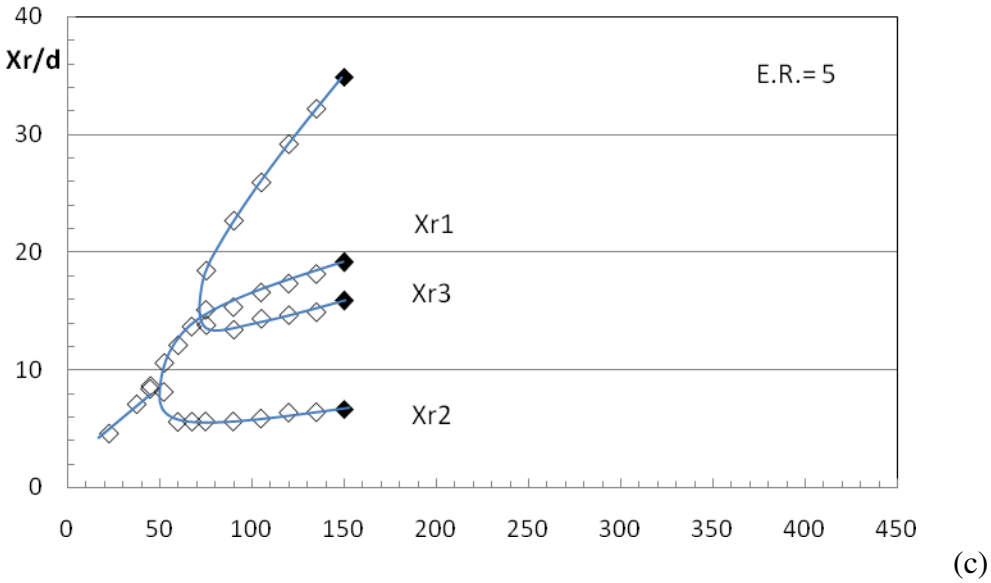

(c)

FIGURE 4: Reattachment lengths with Reynolds number for E.R=2, 3 and 5, lines are just for visual help, filled dots represent the 9 randomly chosen cases by the simulator for testing.

4.2 ANN data preparation, network training, validation, testing and results

Before the ANN model can be used to provide the desired output, the model needs to be trained to recognise the relationships between the input (Re and E.R.) and the desired attachment positions (Xr1, Xr2, Xr3, and Xr4). These relationships will be stored as connection weights between the different neurones. The process of determining the weights is called the training or the learning process. Prior to conducting the training process, a set of input-output patterns are first prepared. The data set used in the development of this model was taken from the results of the extensive CFD calculations for the expansion ratios of 2, 3, and 5 respectively of figure 4. The data set consisted of 44 cases or data sets. 35 of these cases were used for model development and training while the remaining 9 cases, shown as filled dots on figure 4 (20%) of the data set were used to evaluate the developed model performance. These nine cases were selected randomly from the data set, but were chosen to be representative of the span of the

Reynolds numbers at hand and the three expansion ratios. The multi-layer feed-forward network used in this work was trained using the Back-propagation (BP) paradigm developed by Rumelhart and McClelland [14]. Simpson [15] gives a different equation that provides a generalised description of how the learning and recall process is performed by the BP algorithm.

The training process of this ANN model was performed using the *NeuroShell*^{TM} simulator. After completing 180429 epoch, the network converged to a threshold of 10^{-5} . The network model goodness of fit, R^2 (R^2 is defined as the coefficient of determination), demonstrated that the developed ANN model produced attachment positions that were in close agreement with the actual values. The R^2 values of the outputs Xr1, Xr2, Xr3, and Xr4 were 0.8617, 0.8325, 0.9397 and 0.9682 respectively. Having trained the network successfully, the next step is to test the network's generalisation capability using a different data set in order to judge its performance.

Using the 9 cases that were randomly selected from the data set, the developed model was tested to assess its generalisation capabilities. The R^2 values for the Xr1, Xr2, Xr3, and Xr4 were 0.9383, 0.8577, 0.997 and 0.999 respectively. Figures 5(a, b, c, d) and 6 (a, b, c, d) illustrate the relationship between actual and predicted attachment positions of Xr1, Xr2, Xr3, and Xr4 for the training data and the testing data sets respectively.

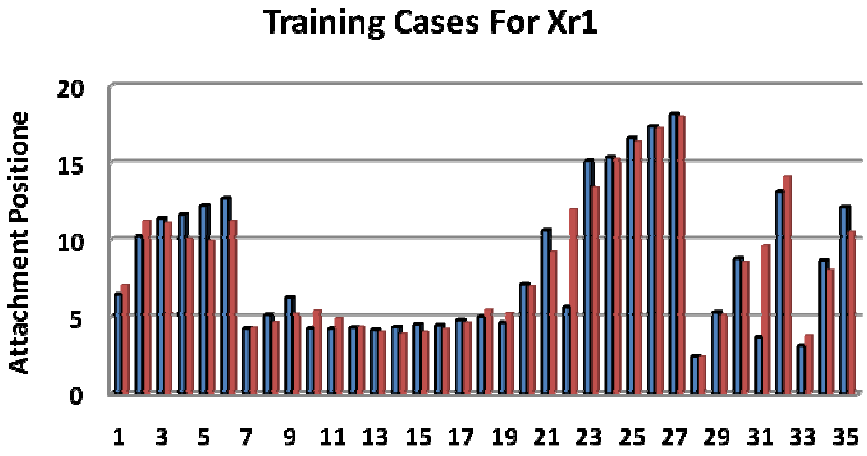

FIGURE 5a: Actual vs. Predicted Results for the output Xr1 in the Developed ANN Model.

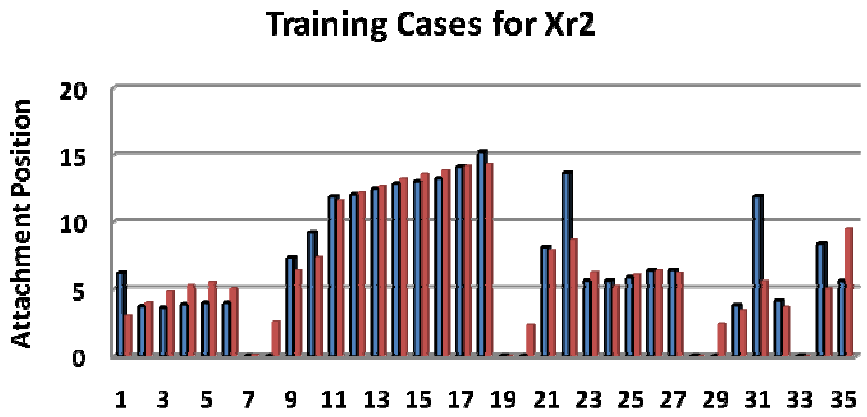

FIGURE 5b: Actual vs. Predicted Results for the output Xr2 in the Developed ANN Model.

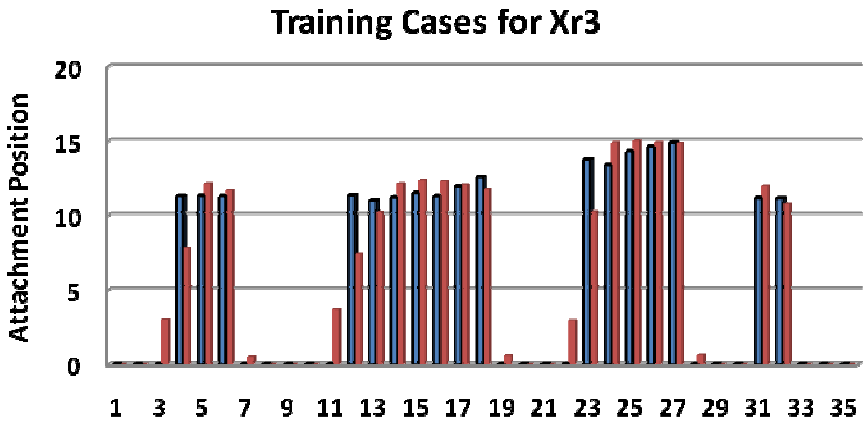

FIGURE 5c: Actual vs. Predicted Results for the output Xr3 in the Developed ANN Model.

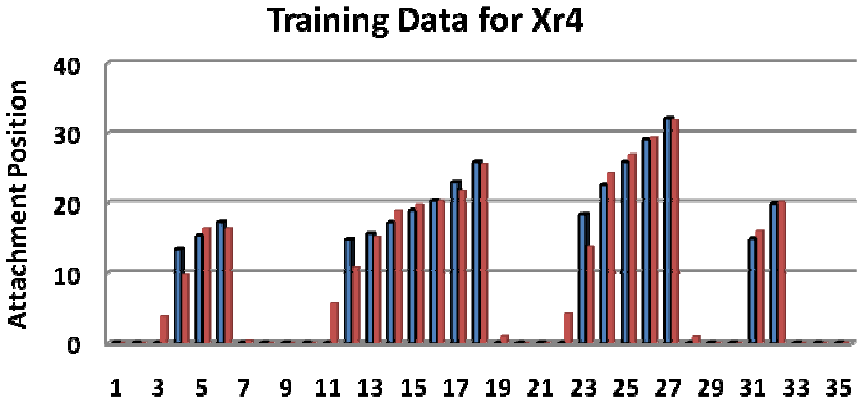

FIGURE 5d: Actual vs. Predicted Results for the output Xr4 in the Developed ANN Model.

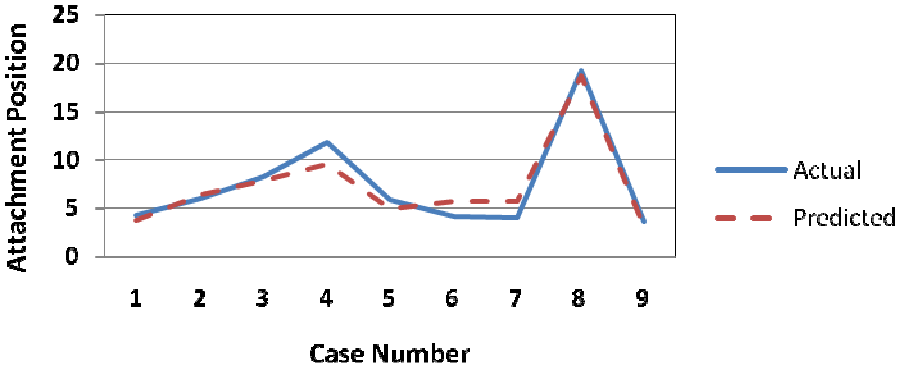

FIGURE 6a: Actual vs. Predicted attachment position for Xr1 in the Testing Cases.

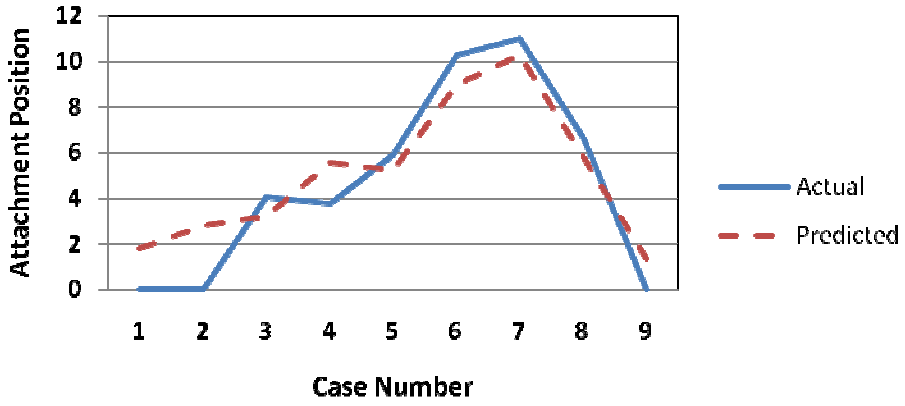

FIGURE 6b: Actual vs. Predicted attachment position for Xr2 in the Testing Cases.

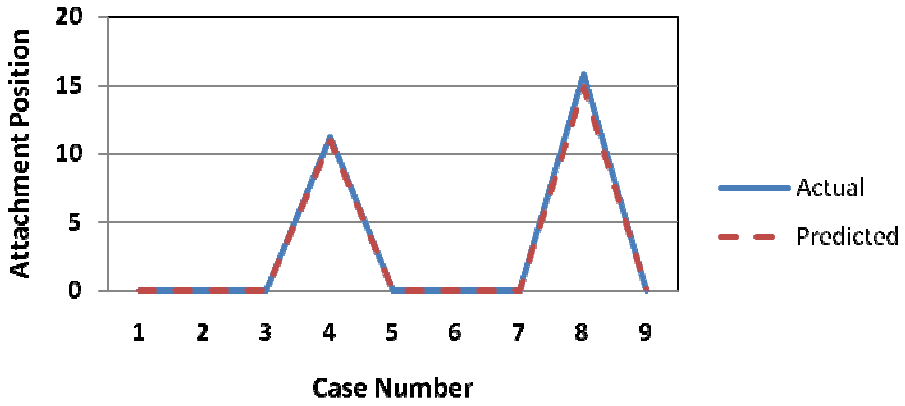

FIGURE 6c: Actual vs. Predicted attachment position for Xr3 in the Testing Cases.

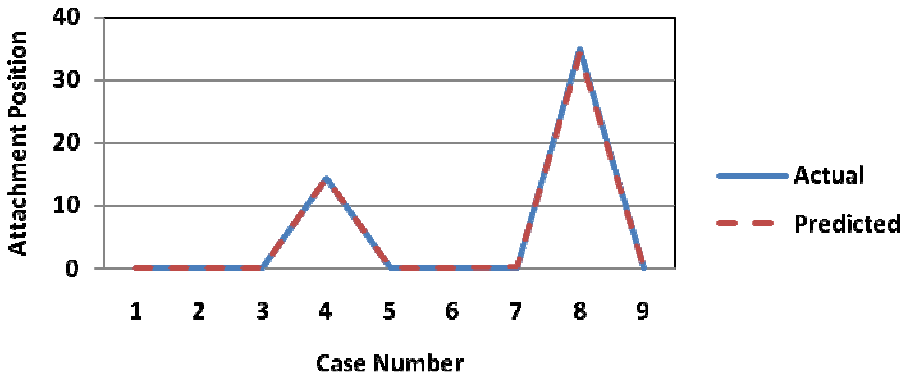

FIGURE 6d: Actual vs. Predicted attachment position for Xr4 in the Testing Cases.

Examination of the results obtained from the testing set of ANN model, suggests that there are very close agreement between actual and predicted values for the attachment positions Xr2, Xr3, and Xr4 and a moderate agreement for Xr1. As shown in figure 6a the predicted attachment position for Xr2 differ slightly from the actual attachment position, the predicted value in case 1 was 1.81 while the actual was 0.0, similarly there was small difference in the predicted value of the second testing case the actual was 0.0 while the ANN model predicted 2.82. All the other

seven cases predictions are in close agreement with the actual attachment position the R^2 value for Xr2 was 0.8577. For Xr1 the results are shown in figure 6a. The testing results indicates that Xr1 was predicted with higher accuracy the R^2 value is 0.9383 which indicate that 93.83 percent of the variation in the data provided can be explained by the two input given and the developed model. Figures 6c and 6d outlined the highly accurate prediction of attachment position for Xr3 and Xr4 when compared with actual results. The R^2 value was 0.997 and 0.999 for Xr3 and Xr4 respectively.

Intensive double precision (because of small magnitude of numbers) computations are necessary to obtain the CFD solutions. For a single Reynolds number as long as 27 hours of computing time are necessary to reach a converged solution on a SUN-20 workstation. Hence tremendous effort was necessary to produce the results of figure 3. In addition to being computer intensive, CFD solution provide a large amount of information as part of the solution that has limited usefulness if one is only interested in reattachment lengths. In engineering design where parametric studies are common, time management becomes of primary importance. The present study has shown that in the case of laminar flows through plane sudden expansions, it is only necessary to obtain CFD solutions for a limited number of Reynolds numbers. An ANN model can then be trained to reproduce with good accuracy the variation of reattachment length with Reynolds number. These results indicate that reattachment positions can be predicted instantly with good accuracy for any E.R between 2 and 5 and Re value between 0.0 and 400 using the developed ANN model.

5. CONCLUSIONS

Computations were performed using both CFD and ANN. In engineering design where parametric studies are common time management becomes of primary importance. The present study has shown that in the case of laminar flows through plane sudden expansions, it is only necessary to obtain CFD solutions for a limited number of Reynolds numbers and expansion ratios. An ANN model can then be trained to reproduce with good accuracy the variation of reattachment length with Reynolds number and expansion ratio. The time needed to develop and test the ANN model is very short; if the data are available, and the person is experienced and familiar with the ANN software, model development and testing can be accomplished in approximately one hour or two. If the model was already developed and only some new data to be tested or changes are needed to be performed on the model, then it is a matter of very few minute. Neural networks offer a number of advantages, including shorter modelling time, less formal statistical training requirements, ability to implicitly detect complex nonlinear relationships between dependent and independent variables, ability to detect all possible interactions between predictor variables, and the availability of multiple training algorithms. Artificial neural networks models also allow fast processing of large amounts of information. Their generalisation capability makes them more robust to noise.

6.REFERENCES

1. F. Durst, J. F.C. Pereira, C. Tropea. *"The plane symmetric sudden-expansion flow at low Reynolds numbers".* J. Fluid Mechanics, 248:567-581, 1993

2. W. Cherdron, F. Durst, J. H. Whitelaw. *"Asymmetric flows and instabilities in symmetric ducts with sudden expansions".* J. Fluid Mechanics, 84:13-31, 1974

3. R.M. Fearn, T. Mullin, K.A. Cliffe, K. *"Non-linear flow phenomena in a symmetric sudden expansion".* J. Fluid Mechanics, 211:595-608, 1990

4. F. Battaglia, S. J. Tavener, A. K. Kulkarni, C. L. Merkle. *"Bifurcation of low Reynolds number flows in symmetric channels".* AIAA J., 35:99-105, 1997

5. B. P. Leonard. *"A stable and accurate connective modelling procedure based on quadratic upstream interpolation".* Comput. Methods Appl. Mech. Eng., 19:59-98, 1979

6. R.I. Issa. *"Solution of the implicitly discretised fluid flow equations by operator splitting".* J. Comput. Phys., 62:66-82, 1996

7. S. S. S. Sakla. *"Neural network modelling of the load-carrying capacity of eccentrically-loaded single angle strut".* Journal Constructional Steel Research, 60:965-987, 2004

8. H.S. Stern. *"Neural networks in applied statistics".* Proceedings of the statistical computing section. American Statistical Association, pp.150-154, 1991

9. K.B. DeTienne, D. H., DeTienne, L. W., Lewis. *"Artificial neural networks for the management researchers: the state of the art".* Research Report, Department of Organizational Leadership and Strategy, Brigham Young University, 2003

10. W.C. Carpenter, M.E. Hoffman. *"Training Back-Propagation Neural Networks".* AI Expert, 10:30-33, 1995

11. Lapeds, R. Forber. *"How Neural Network Works".* Neural Information Processing Systems, American Institute of Physics, pp.442-456, 1988

12. R. Hecht-Nielsen. *"Theory of Backpropagation Neural Network".* Proc. Int. Joint Conf. on Neural Networks, IEEE, Washington, D.C., 1:593-605, 1989

13. Y. Ouwa, M. Watanabe, H. Asawo. *"Flow visualisation of a two-dimensional water jet in a rectangular channel".* Japanese J. of Applied Physics, 20:243-247, 1981

14. D. E. Rumelhart, J. L. McClelland. In: Parallel Distributed Processing: Exploration in the Microstructure of Cognition, Foundations, MIT Press, Cambridge, Massachusetts, (1986)

15. P.K. Simpson. *"Artificial Neural Systems: Foundations, Paradigms, Applications, and Implementations",* Pergamon Press, first edition, Elmsford, New York, (1990)

Allowable Differential Settlement of Oil Pipelines

Zahra Faeli afs_faeli@yahoo.com
Researcher/ Faculty of Civil Engineering
University of Tehran Tehran,
1779816691,Iran.

Ali Fakher afakher@ut.ac.ir
Associate Professor / Faculty of Civil Engineering
University of Tehran Tehran,
1779816691,Iran.

Seyed Reza Maddah Sadatieh srmaddah@ut.ac.ir
Assistant Professor / Faculty of Engineering Science
University of Tehran Tehran,
1779816691,Iran.

Abstract

The allowable settlement of pipelines has been mentioned rarely in design references and codes. The present paper studies the effects of differential settlement of pipeline bed on resulted forces and deformations and then determines the allowable differential settlement of pipelines in two conditions as follows: (i) heterogeneous soil bed and (ii) adjacent to steel tanks. To accomplish the studies, numerical simulation of pipeline is used. The pipeline bed is idealized by Winkler springs and four-element standard viscoelastic Burger model. Also, the use of geosynthetic reinforcement is studied in heterogeneous soil beds and the effect of geosynthetics on decreasing the settlement is investigated. The pipeline-tank joints in two cases of fixed and flexible joints are investigated and the results for two kinds of joints are compared.

Keywords: Allowable differential settlement, Burger model, Fixed joint, Flexible joint, Geosynthetic.

1. INTRODUCTION

The values of allowable settlement of pipeline have been discussed rarely in pipeline design references and this subject has been challenged geotechnical and pipeline engineers. Discussions about allowable settlement of pipelines were propounded for pipelines constructed in permafrost zone and exposed to thaw differential settlement [1] & [2]. Also, investigations have been proposed about evaluation of deformations and generated forces of pipelines exposed to settlement of soil bed [3] & [4] . Moreover, studies to analysis the deformations of pipeline due to settlement of other equipments were accomplished [5]. But such a comprehensive study has yet not been made to determine the quantitative and qualitative values of allowable differential settlement of pipelines.

2. STATEMENT OF THE PROBLEM

There are various conditions to generate the differential settlement of pipeline. In proposed research, some prevalent states are studied.

2.1. Pipeline Resting on Heterogeneous Soil Bed

Figure (1) shows schematically the pipeline and it's soil bed (Burger model). The pipeline passed from a loose bed. It's assumed the intermediate loose bed is composed of soft clayey deposit and exposed to instantaneous settlement, primary consolidation and creep due to applied loading. The ground foundation around loose clay bed is composed of dense granular soil that only is exposed to finite instantaneous settlement. The pipeline diameter and thickness are D and t, respectively. Loads applied on pipeline are the weight of steel materials, transitional oil media, soil surcharge over the pipeline and the pressure of internal fluid.

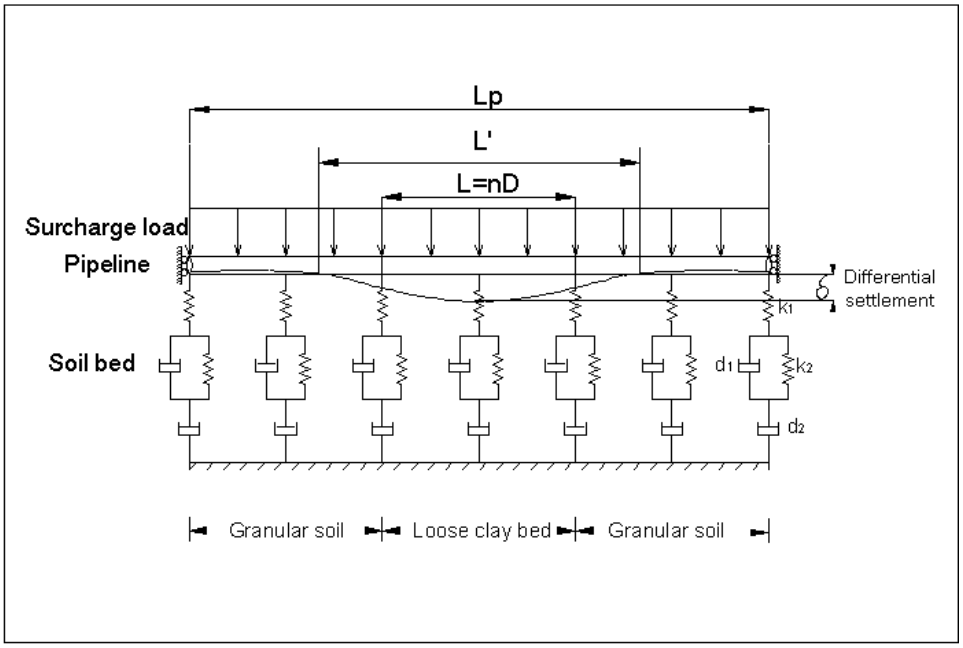

FIGURE 1: Schematic sketch of pipeline resting on heterogeneous bed

2.2. The Use of Geosynthetic Reinforcement in Pipeline Bed

To decrease the differential settlement of pipeline resting on heterogeneous beds, a geosynthetic layer with specified tensile strength is entered the model. In the model of geosynthetic-reinforced bed, a dense sandy layer (by Winkler springs elements) is placed beneath the pipeline and over the heterogeneous bed and geosynthetic layer is lied at the interface of two soil layers. Figure (2).

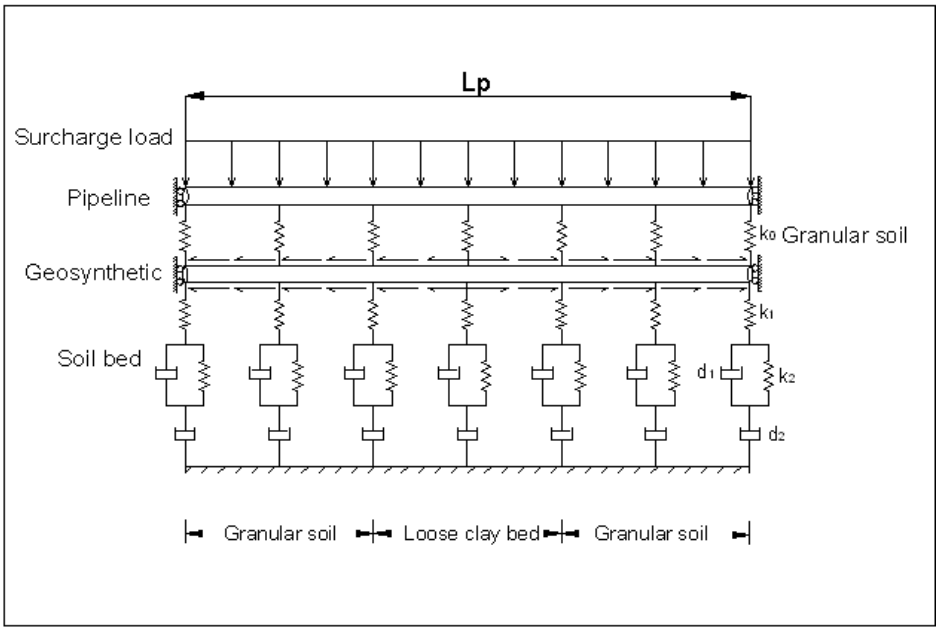

FIGURE 2: Schematic sketch of geosynthetic-reinforced bed beneath the pipeline

2.3. Pipeline Adjacent to Tank

The schematic sketch of pipeline adjacent to tank is shown in Figure (3). This condition is very practical in oil industry. The pipeline bed is idealized by Winkler spring elements. The distance of first sleeper beneath the pipeline from tank is specified as a function of pipe diameter (L_t=nD). Two kinds of joints are used practically to attach the pipeline to tanks: (i) fixed joint and (ii) hinge or flexible joint. These kinds are compared in present paper. It's possible to rotate and move vertically at flexible joint whereas the rotations in all directions are restrained at fixed joint. Figure (4) shows an example of flexible joint used in a project in the south of Iran.

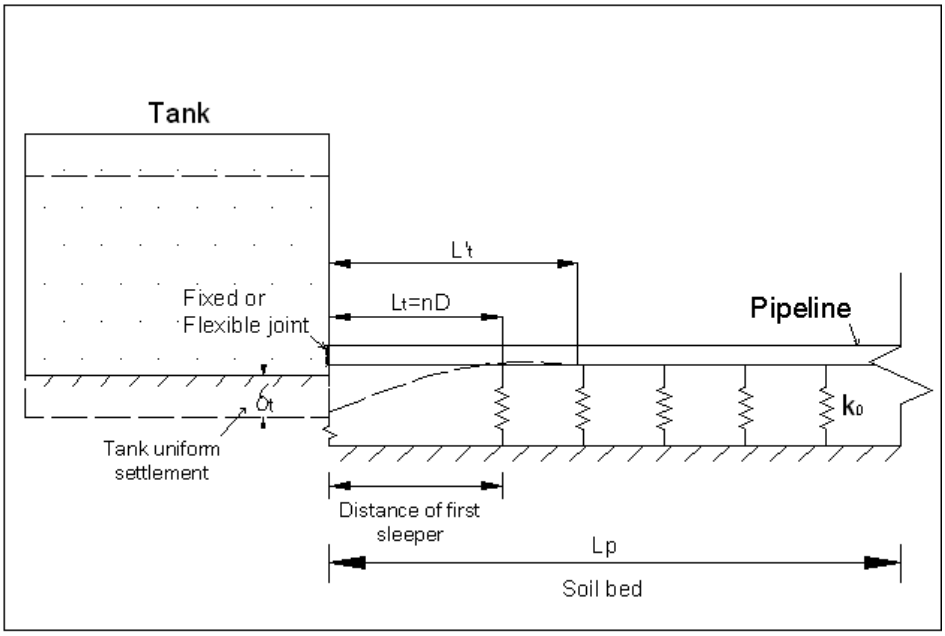

FIGURE 3: Schematic sketch of pipeline adjacent to a tank

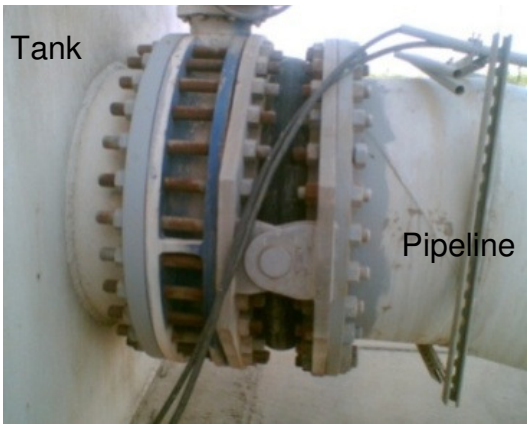

FIGURE 4: Pipeline-tank flexible joint

3. NUMERICAL SIMULATION USED IN RESEARCH

A computer program had been written in ABAQUS [6] finite element software to carry out the studies.

3.1. Simulation of Soil Bed by Burger Model

Idealization of structures beds by lumped parameter elements (spring elements) is considerable in previous investigations [7] but there are few references about the subject of Burger model used in soil beds [8]. This model idealizes primary and secondary (creep) consolidations as well as instantaneous settlement. Each Burger model element is consisted of two spring elements with k_1 and k_2 stiffness coefficients and two dashpot elements with d_1 and d_2 viscous coefficients. The behavior of Burger element exposed to the force of F and resulted deflection of y is stated as equation (1):[9]

$$y = \frac{F}{k_1} + \frac{F}{k_2}\left[1 - \exp\left(\frac{-k_2 t}{d_1}\right)\right] + \frac{Ft}{d_2} \qquad (1)$$

3.2. Pipeline Structure Model

The pipeline is idealized by three dimensional PIPE31 elements in present analyses and the pipe cross sections are selected according to the sections of API-5L-95 code [10] to use standard sections. The hoop stress (σ_h) and equivalent stress (σ_e) are defined as relations (2) and (3), respectively:[11]

$$\sigma_h = \frac{PD}{2t} \qquad (2)$$

$$\sigma_{eqv} = \sqrt{(\sigma_h^2 + \sigma_l^2 - \sigma_h \sigma_l + 3\tau^2)} \qquad (3)$$

Where P= internal pressure, D and t= diameter and thickness of pipeline respectively, σ_l= longitudinal stress and τ=shear stress of cross section. To study the effect of pipeline diameter, the ratio of diameter to thickness (D/t) is considered to be constant approximately in amount of 64.

3.3. Geosynthetic Model

To idealize geosynthetic layer, T3D2 tensile elements are used. To consider frictional strength of between the geosynthetic layer and granular soil (confinement effect) a distributed tensile force is applied over the geosynthetic layer as equation (4).

$$T_g = f\,\gamma_s\,H \quad \left(\frac{kN}{m}\right) \qquad (4)$$

Where Tg= distributed tensile force, f= frictional coefficient (considered in amount of 1), γ_s= soil density (20 kN/m^3) and H=height of soil (1m).

4. THE EFFECTS OF VARIABLES

The effects of variables of Burger model on the values of settlement and resulted forces of pipeline were studied. The stiffness coefficient of spring element as series in Burger model (and stiffness coefficient of Winkler model) is determined by the relation of subgrade reaction modulus according to plate-load test [12]. The spring element of Burger model as series is used to model the instantaneous settlement of bed (relation 5) :

$$k_1 = \frac{E}{D(1-\mu^2)} DL_i \quad \left(\frac{N}{m}\right) \qquad (5)$$

Where D= plate width (pipe diameter), L_i=element length (0.01m), μ=Poisson's ratio of soil (0.5) and E=elasticity module of soil.

To vary the stiffness ratio of dense granular soil to intermediate loose clay soil ($k_1(g)/k_1(c)$) in heterogeneous soil bed showed the differential settlements have increased till $k_1(g)/k_1(c)$=25 and then varied negligibility. Hence, in present study the ratio of $k_1(g)/k_1(c)$ is considered to be 25.The studies showed to select the coefficients of k_2, d_1 and d_2 as very large for around dense soil resulted in only instantaneous settlement. These variables for intermediate loose clay soil were determined so that maximum long term settlement would be arised in various amounts of loose bed lengths. In this way, minimum values are obtained for allowable settlement of pipelines on heterogeneous beds.

The studies showed $k_2=k_1/100$ resulted in maximum long term settlement of pipeline. The variable of k_2 in equation (1) is used to model the primary consolidation settlement. The primary consolidation values of bed due to various pipeline loads were obtained from used Burger model and Terzaghi relation as Figure (5). To compare the settlements of Burger model with Terzaghi relation resulted in calibrated parameter of Burger model (k_2) that is stated as equation (6). This relation is used to determine the variable of k_2 for various diameters of pipelines. The settlements resulted from Burger model with calibrated variable of k_2 are in good agreement with settlements calculated by Terzaghi relation as Figure (5).

$$k_{2(D)} = \frac{D}{0.508} \times {}^{k_1}/_{100} \quad \left(\frac{N}{m}\right) \qquad (6)$$

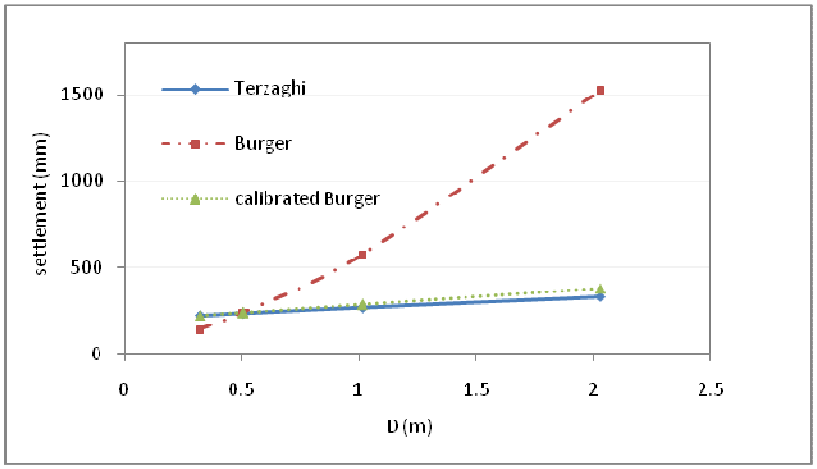

FIGURE 5: Comparison of settlement of Burger model with Terzaghi equation and correction of Burger model

Also, parametric studies for various diameters of pipelines and lengths of loose clay bed showed the ratio of (d_1/d_2) in Burger model is effective on time required for final settlement and consequently is effective on differential settlement values at analysis time. d_1 and d_2 are viscous variables of Burger model that correlate to time dependent variables of soil settlement.

Numerous studies about effects of variables of pipeline settlement were accomplished. Maximum values of differential settlement (δ_{max}), longitudinal stress resulted from settlement ($\sigma_{L,max}$), equivalent stress ($\sigma_{e,max}$), longitudinal strain ($\varepsilon_{L,max}$) and bending moment (M_{max}) were determined for various loose bed length (L) and pipeline diameter (D). The Figures (6) show the variation of (δ_{max}) and ($\sigma_{L,max}$) with (L/D) for various diameters of pipeline.

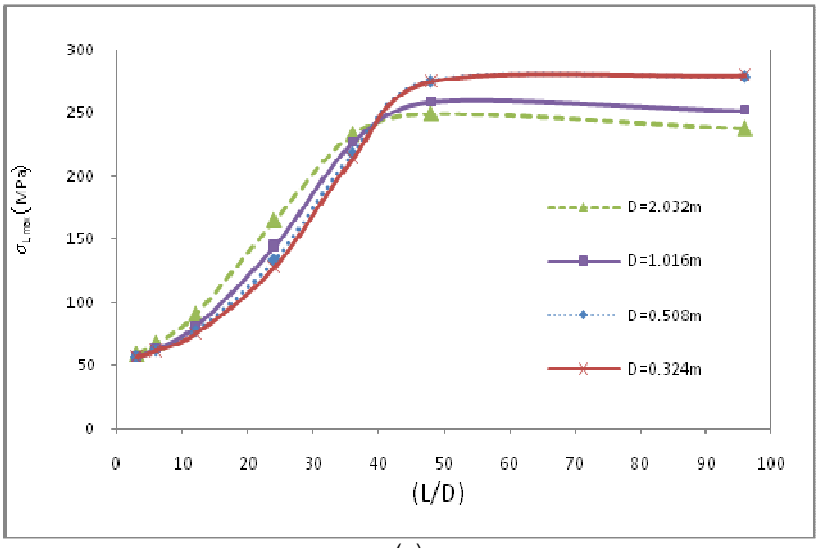

(a)

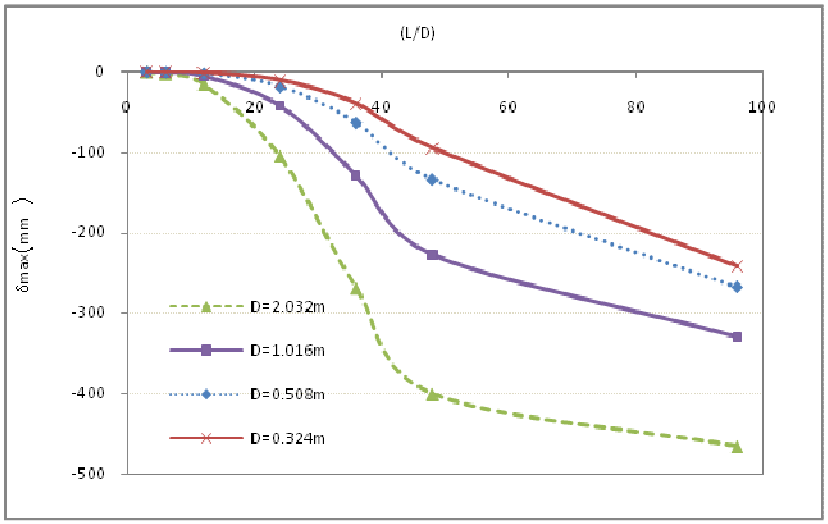

(b)

FIGURE 6: Variation of (a) max longitudinal stress and (b) max differential settlement with the ratio of loose bed length to pipeline diameter

Also, maximum values of stress-strain and bending moment due to varied settlement of tank (δ_t) were obtained for fixed and flexible joints of pipelines and various sleeper distances (L_t). The Figure (7) shows the effect of sleeper distance on longitudinal stresses of a pipeline with fixed joint. To increase the sleeper distance results in less stresses-strains.

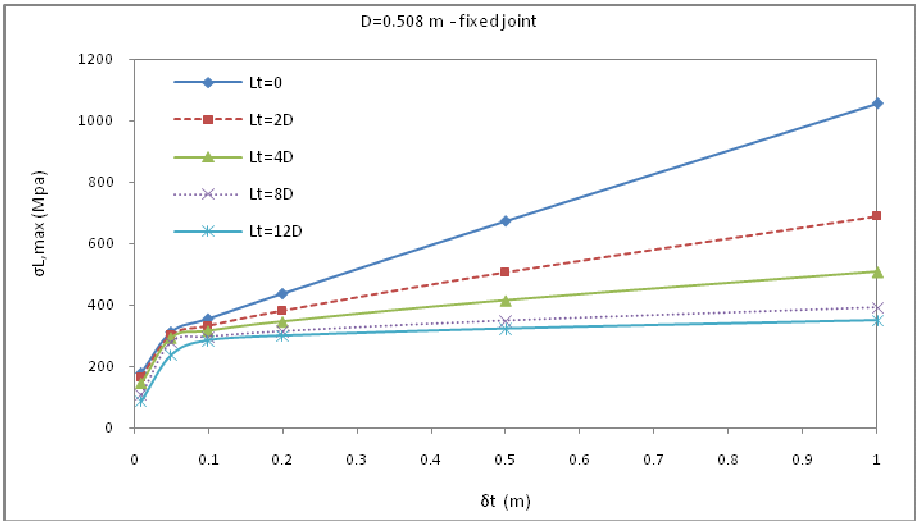

FIGURE 7: Effect of sleeper distance on max longitudinal stress with tank settlement (δt)

The other studies show to use of geosynthetic reinforcement causes to decrease the settlement of pipeline bed and resulted forces as Figure (8).

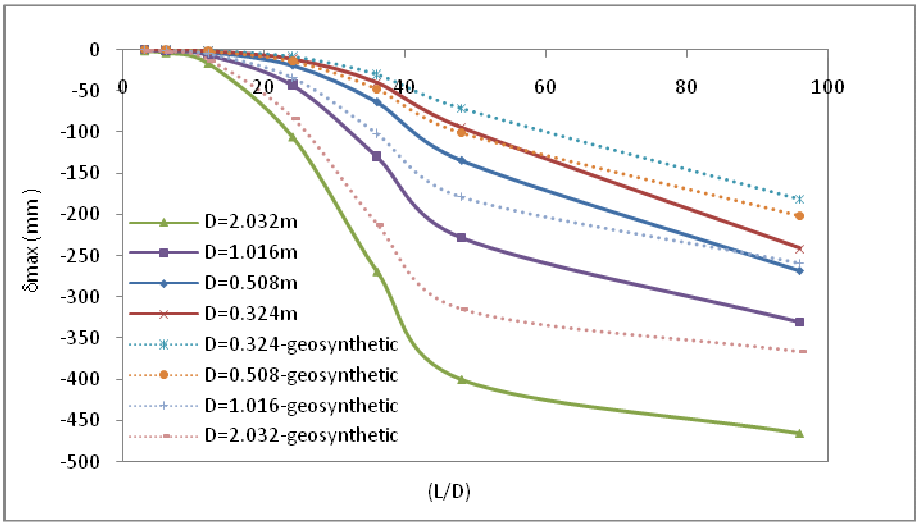

FIGURE 8: The effects of geosynthetic layer on differential settlement of pipeline with the ratio of loose bed length to pipeline diameter (L/D)

5. DISCUSSION ABOUT ALLOWABLE SETTLEMENT OF PIPELINES

5.1. The Criteria for Limiting the Settlement

The present paper aim is to suggest allowable differential settlement of pipelines. To limit the settlement, various criteria could be used. Stress and strain are two main criteria for limiting the pipeline settlement. Historically, the most codes of pipelines have used the allowable stress-based design methods to design the pipelines against applied forces. In the half of the '90 ies limit state design methods entered the pipeline design codes. In this way, to define failure states of pipelines has provided the possibility of more efficient and economic designs. The limit state design methods use limited strains and bending moments moreover the limited stresses.

(i). Allowable stress method:

For this method in present research the design factors were used from ABS2000 code [13]. This code limits the hoop stresses, longitudinal and equivalent stresses to 72%, 80% and 90% specified minimum yield stress (SMYS), respectively.

(ii). Bending moment capacity method:

The bending moments of pipeline were controlled by this method. Maximum allowable bending moment of pipeline ($M_{Allowable}$) is determined according to the proposed relation of reference [14].

(iii). Allowable strain method:

The critical compression strain of pipeline materials (ε_c^{crit}) would be estimated by using empirical equation according to CSA-Z662 code [15]. The limit state of plastic failure of welds is initiated from the cracks of weld surface due to tensile strains. Many of codes consider the value of 2% as allowable tensile strain [16].

As settlement increases, the above mentioned three criteria would happen respectively. See Figure (9).

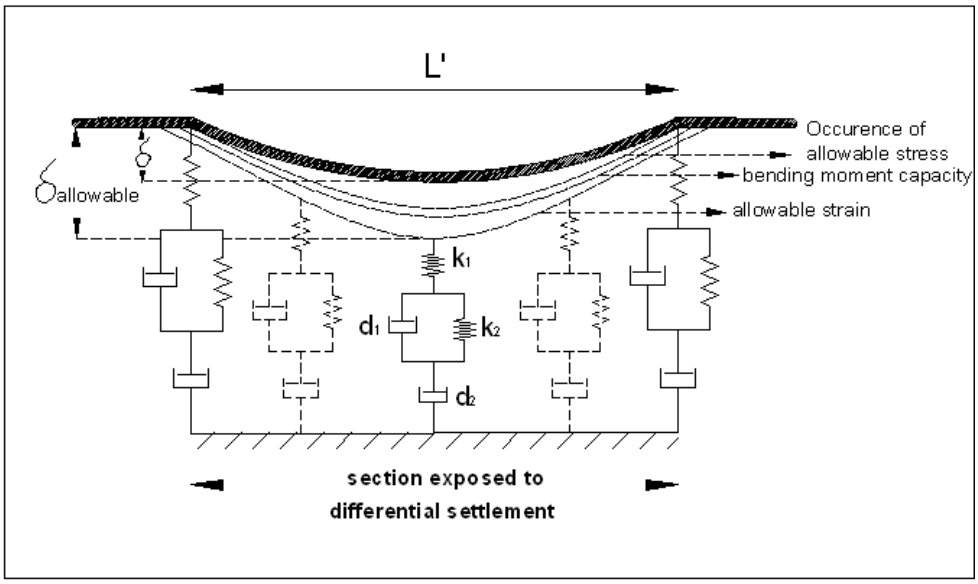

FIGURE 9: Determination of allowable differential settlement of pipeline

5.2. The Allowable Differential Settlement of Pipelines on Heterogeneous Soil Bed

After many analyses, allowable differential settlement of pipeline is estimated by comparing the resulted forces and stress-strain surface due to settlement with allowable limits (Section 5.1). The values of allowable differential settlement on the basis of used methods are summarized as Table (1). As an example, for determining the allowable differential settlement by the method of allowable longitudinal stress, the length of loose bed is increased till the longitudinal stresses of pipeline due to settlement reach to allowable limit and then the maximum differential settlement corresponding to allowable longitudinal stress is considered as allowable differential settlement of pipeline($\delta_{allowable}$). The analyses were accomplished for some pipelines with various diameters and it's observed the allowable differential settlements of pipelines were 0.09D by using the allowable longitudinal stress method, Figure(6).The results were determined for D/t=64 but these are acceptable for D/t<64, overestimately.

Relative conditions	Control method	Allowable differential settlement ($\delta_{allowable}$)
Conservative	Allowable equivalent stress	0.08D
	Allowable longitudinal stress	0.09D
Moderate	Bending moment capacity	0.12D
Most economic	Allowable compression strain	0.8D

TABLE 1: Allowable differential settlements of pipelines resting on heterogeneous soil beds

The allowable settlement values of 0.08D, 0.09D, 0.12D and 0.8D, are obtained in loose bed lengths of 29D, 31D, 35D and 105D, respectively. If the length of loose bed is less than mentioned values, then the pipeline settlement is less than allowable amount in any soil

conditions. if the loose bed length is more than them, the above table values are accepted as minimum allowable differential settlements. It should be explained the variables of Burger model were determined so that the maximum settlements of bed were resulted. If the soil bed conditions are improved then allowable limits of moment/stress-strain would be happen in larger loose bed lengths and more values of differential settlement than above values would be resulted.

By using Table (1), a designer engineer could determine allowable settlements of a pipeline according to pipeline diameter and length of loose bed.

5.3. The Allowable Differential Settlement of Pipelines Adjacent to Tanks

To determine the allowable settlement, various analyses were accomplished and the results were accumulated. Respect to the flexibility of pipelines, the distance of tank from the first pipeline sleeper has many effects on controlling the settlement values. Hence the allowable differential settlements of pipelines at joint location, are determined as Table (2), according to pipeline diameter, distance of first sleeper from the tank and kind of joint.

Relative conditions	Control method	Distance of first pipeline sleeper from tank (Lt)	Joint kind	Allowable differential settlement ($\delta_{t,allowable}$)	Joint kind	Allowable differential settlement ($\delta_{t,allowable}$)
Conservative	Allowable equivalent stress	0	Fixed	0.015D	Flexible	0.068D
		8D	Fixed	0.030D	Flexible	0.141D
Moderate	Bending moment capacity	0	Fixed	0.029D	Flexible	0.085D
		8D	Fixed	0.09D	Flexible	0.300D
Most economic	Allowable compression strain	0	Fixed	0.034D	Flexible	0.160D
		8D	Fixed	0.107D	Flexible	0.380D
	Allowable tensile strain	0	Fixed	0.059D	Flexible	0.283D
		8D	Fixed	0.175D	Flexible	0.783D

TABLE 2: Allowable differential settlements of pipelines adjacent to tanks

As it's seen from Figure (10), used design method on the basis of considered relative conditions is effective on allowable differential settlements of pipeline ($\delta_{t,allowable}$/D) adjacent to tank.

FIGURE 10: The effect of used design method on allowable differential settlement of pipeline adjacent to tank

The diagrams of Figure (11), show the effect of distance of first sleeper beneath the pipeline (as Lt/D) on allowable settlement values of pipeline at joint location ($\delta_{t,allowable}/D$). The similar results have been obtained for other design methods. Also the effects of using the flexible joints on distributing the resulted forces and increasing the values of allowable settlement, are observed from Figures (10) and (11).

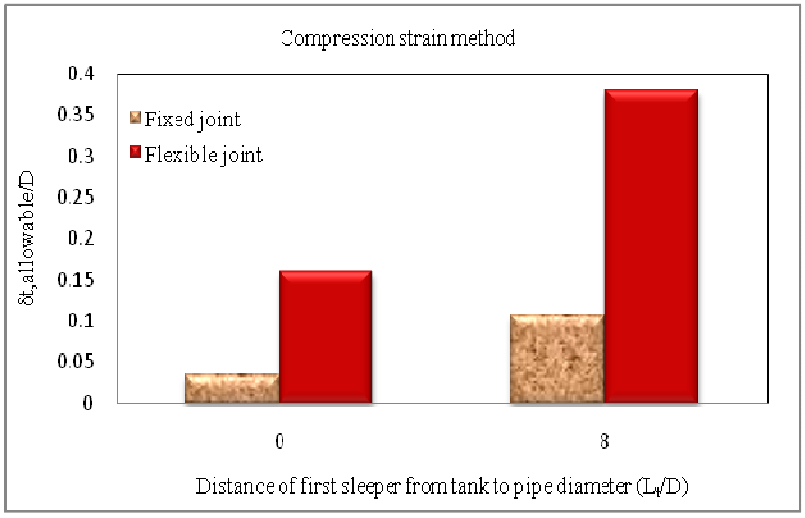

FIGURE 11: The effect of sleeper distance on allowable differential settlement of pipeline adjacent to tank

6. CONCLUSIONS

The paper results are stated as follows:

1. The allowable differential settlements of pipelines are proposed as Table (1) and Table (2). These tables are useful for geotechnical designer engineers to decide about the values of allowable settlement in a project.

2. According to Figure (8), using of geosynthetic layer is effective on decreasing the settlement values and resulted forces of pipelines. This effect has been more observed in loose bed length of about L=24D. Also, beneficial effects of geosynthetic are observed for smaller diameters of pipelines.

3. As the distance of first sleeper from tank (L_t) increases, the values of resulted forces of pipeline from settlement decrease considerably.

4. Using of flexible joint and placement of first sleeper in distance of (L_t=8D), cause a considerable increasing of allowable differential settlement of pipeline.

5. The ratio of loose bed length to pipe diameter (L/D) is effective on the value of differential settlement. As the ratio of (L/D) increases the values of differential settlement and resulted forces of pipeline increase, too.

6. In the same ratio of loose bed length to diameter (L/D), increasing of pipeline diameter will increase the differential settlement of pipeline.

7. For pipeline adjacent to tank, the resulted forces and stresses-strains increase due to increase the tank settlement (δ_t). Also, by decreasing the pipeline diameter (D) in the same settlement of tank, the resulted forces and stress-strain values increase.

Proposal allowable settlements as indicated in Table (1) and (2) could be considered as the main achievements of this paper.

The above mentioned conclusions could be used by designer engineers to determine allowable settlement and also to understand the governing parameters.

7. REFERENCES

1) Nixon, J.F., Sortland, K.A., James, D.A., " Geotechnical aspects of northern gas pipeline design", 5TH Canadian Permafrost Conference, Collection Nordicana No. 54, Laval University, Montreal, Quebec, Canada, 1990.
2) Lee, D., Kang, J.M., C., K., " Comparison of characteristics of arctic, marine, and desert areas for designing pipeline network systems", 5TH International Conference on Northeast Asian, Russia,1999.
3) Limura, S.," Simplified mechanical model for evaluating stress in pipeline subject to settlement", JCBM, Elsevier, 18 (6):119-129 ,2004.
4) Dimov, L. A., Bogushevskaya, E. M., "Application of theory of beam analysis for arterial oil pipelines across swamps", Soil Mechanics and Foundation Engineering, 39(4):139-143, 2002.
5) Kellezi, L., Kudsk, G., Hansen, P.B., " FE modelling of spudcan-pipeline interaction", Proc. ISFOG 2005, Perth, Australia, pp. 551-557, 2005.
6) Hibbit,H. D., Karlsson, B. I. and Sorensen, P., "ABAQUS/Standard Theory Manual version 6.5", Karlsson and Sorensen Inc (HKS), 1998.

7) Einsfeld, R. A., Murray, D. W., Yoosef-Ghodsi N., “Buckling analysis of high-temperature pressurized pipelines with soil-structure interaction”, Brazilian Society of Mechanical Sciences and Engineering, 25(2):164-169, 2003.
8) Dey, A., Basudhar, P,K.,”Flexural response of surface strip Footings resting on reinforced viscoelastic foundation beds”, IGC Bangalore,2008.
9) Goodman, R., “ Introduction to Rock Mechanics”, 2th Edition, Wiley Book Company, New York, pp.202-217, 1989.
10) API, “American Petroleum Institute Publishing Services”, Specification 5L for Line Pipe, Washington, DC,USA, 1995.
11) Powers, J.T., Dalton, P., Aybinder, A., “ International pipeline design code comparisons and the trend towards limit state design”, Pipeline Terminal and Storage Conference, Houston, Texas ,1996.
12) Bowels, J.E.,“ Foundation Analysis and Design”, 4th Edition, MC Graw Hill Book Company, New York, pp. 501-506, 1998.
13) ABS,” Guide for Building and Classing Undersea Pipelines and Risers”, American Bureau of Shipping, 2000.
14) Bai, Y., “ Pipelines and Riseres”, Elsevier Ocean Engineering Book Series, pp. 67-70, 2003.
15) CSA, “Canadian Standards Association”, Z662: Oil and Gas Pipeline Systems, Exdale, Ontario, Canada, 2007.
16) Lio, B., Liu, X.J., Zhang, H. , “ Strain-based design criteria of pipelines”, Journal of Loss Prevention in the Process Industries, Vol. 22: 884-888, 2009.

CALL FOR PAPERS

Journal: International Journal of Engineering (IJE)
Volume: 4 **Issue:** 5
ISSN: 1985-2312
URL: http://www.cscjournals.org/csc/description.php?JCode=IJE

About IJE

International Journal of Engineering (IJE) is devoted in assimilating publications that document development and research results within the broad spectrum of subfields in the engineering sciences. The journal intends to disseminate knowledge in the various disciplines of the engineering field from theoretical, practical and analytical research to physical implications and theoretical or quantitative discussion intended for both academic and industrial progress.

Our intended audiences comprises of scientists, researchers, mathematicians, practicing engineers, among others working in Engineering and welcome them to exchange and share their expertise in their particular disciplines. We also encourage articles, interdisciplinary in nature.

To build its International reputation, we are disseminating the publication information through Google Books, Google Scholar, Directory of Open Access Journals (DOAJ), Open J Gate, ScientificCommons, Docstoc and many more. Our International Editors are working on establishing ISI listing and a good impact factor for IJE.

IJE List of Topics:

The realm of International Journal of Engineering (IJE) extends, but not limited, to the following:

- Aerospace Engineering
- Agricultural Engineering
- Biomedical Engineering
- Chemical Engineering
- Civil & Structural Engineering
- Computer Engineering
- Control Systems Engineering
- Education Engineering
- Electrical Engineering
- Electronic Engineering
- Engineering Mathematics
- Engineering Science
- Environmental Engineering
- Fluid Engineering
- Geotechnical Engineering
- Industrial Engineering
- Manufacturing Engineering
- Materials & Technology Engineering
- Mechanical Engineering
- Mineral & Mining Engineering

- Nuclear Engineering
- Petroleum Engineering
- Telecommunications Engineering
- Optical Engineering
- Robotics & Automation Engineering

Important Dates

Volume: 4
Issue: 5
Paper Submission: September 30 2010
Author Notification: November 01, 2010
Issue Publication: November / December 2010

CALL FOR EDITORS/REVIEWERS

CSC Journals is in process of appointing Editorial Board Members for ***International Journal of Engineering (IJE)***. CSC Journals would like to invite interested candidates to join **IJE** network of professionals/researchers for the positions of Editor-in-Chief, Associate Editor-in-Chief, Editorial Board Members and Reviewers.

The invitation encourages interested professionals to contribute into CSC research network by joining as a part of editorial board members and reviewers for scientific peer-reviewed journals. All journals use an online, electronic submission process. The Editor is responsible for the timely and substantive output of the journal, including the solicitation of manuscripts, supervision of the peer review process and the final selection of articles for publication. Responsibilities also include implementing the journal's editorial policies, maintaining high professional standards for published content, ensuring the integrity of the journal, guiding manuscripts through the review process, overseeing revisions, and planning special issues along with the editorial team.

A complete list of journals can be found at http://www.cscjournals.org/csc/byjournal.php. Interested candidates may apply for the following positions through http://www.cscjournals.org/csc/login.php.

Please remember that it is through the effort of volunteers such as yourself that CSC Journals continues to grow and flourish. Your help with reviewing the issues written by prospective authors would be very much appreciated.

Feel free to contact us at coordinator@cscjournals.org if you have any queries.

Contact Information

Computer Science Journals Sdn BhD
M-3-19, Plaza Damas Sri Hartamas
50480, Kuala Lumpur MALAYSIA

Phone: +603 6207 1607
+603 2782 6991
Fax: +603 6207 1697

BRANCH OFFICE 1
Suite 5.04 Level 5, 365 Little Collins Street,
MELBOURNE 3000, Victoria, AUSTRALIA

Fax: +613 8677 1132

BRANCH OFFICE 2
Office no. 8, Saad Arcad, DHA Main Bulevard
Lahore, PAKISTAN

EMAIL SUPPORT
Head CSC Press: coordinator@cscjournals.org
CSC Press: cscpress@cscjournals.org
Info: info@cscjournals.org

COMPUTER SCIENCE JOURNALS SDN BHD
M-3-19, PLAZA DAMAS
SRI HARTAMAS
50480, KUALA LUMPUR
MALAYSIA